

Quantifying the Findability of Fishways by Computational Fluid Dynamics

A Case Study of Weir Grave in the River Meuse



Quantifying the Findability of Fishways by Computational Fluid Dynamics

A Case Study of Weir Grave in the River Meuse

Author(s)

Sam Majvis

Tom O'Mahoney

Cover photo

© Rijkswaterstaat | Joop van Houdt

Quantifying the Findability of Fishways by Computational Fluid Dynamics

A Case Study of Weir Grave in the River Meuse

Client	Rijkswaterstaat Zuid-Nederland District Noord-Brabant, hoofdkantoor Den Bosch
Contact	Frank Collas
Reference	Projectplan - SITO Programmasubsidie IenW 2024 WVH 01 2024 - Rivierkundig onderzoek
Keywords	Computational Fluid Dynamics, CFD, fish migration, fish passage, fishway, findability, weir, Meuse

Document control

Version	1.0
Date	05-12-2024
Project nr.	11210364-010
Document ID	11210364-010-ZWS-0001
Pages	47
Classification	
Status	final

Author(s)

	Sam Majvis	Tom O'Mahoney

Summary [EN]

Developing effective fishways requires knowledge of fish behaviour and hydraulic engineering in equal measures. Many hydraulic structures in the Netherlands are aging and due replacement, meaning that many new designs will be made in the coming decades. Ecologists and engineers must work together to determine the hydraulic conditions that will result in a successful weir and fishway design. Field observations are, understandably, the golden standard for ecological research on fish behaviour. For weirs, fishways and other hydraulic structures that have not been built yet, however, we need another way to research their effectiveness for fish migration. This report demonstrates the capabilities of Computational Fluid Dynamics (CFD) to fulfil this need by means of a case study of weir Grave in the river Meuse.

By quantifying the needs of a set of target fish species, designs of future structures can be optimized prior to implementation, as opposed to retrofitting a solution, as was the case for the current weirs in the Meuse. Fishway effectiveness consists of multiple aspects: findability, accessibility, passability and the total time spent. The findability of the entrance of a fishway is the essential first step a fishway's total effectiveness, as a fishway that cannot be found, definitely cannot be passed. The focus of this case study is therefore the findability of the fishway at weir Grave.

Two main concepts were considered: the migration limit line and the continuous migration corridor. The migration limit line marks the boundary of a region in which the flow velocity or turbulence becomes too strong to continue swimming upstream. The continuous migration corridor describes the region of conquerable velocities and sufficiently low (passable) turbulence that can be used to successfully migrate upstream. The limits to fish species' swimming performance are available in literature based on field and laboratory observations. Two fish species were analysed as representatives for the weaker and stronger swimmers in the river Meuse: juvenile European eel (glass eel) and adult Atlantic salmon (salmon). Turbulence is very often cited as an important parameter for the findability (and passability) of fishways, but the parameters describing turbulence are very rarely quantified and translated into limits of fish's capabilities, nor are they species-specific.

CFD was successfully applied to quantify the consequences of weir operation for fishway findability. Based on the performed simulations, the findability of the fishway at weir Grave does not seem sufficient for large-scale, successful upstream migration. The fishway is masked by turbulence in almost all simulations. The only scenario with passable turbulence (with 100 m³/s through the weir farthest from the fishway), however, poses other challenges because areas of too low (non-attractive) velocities arise in front of the fishway entrance. For the bottom-dwelling glass eel the continuous migration corridor is very close to the water surface. For salmon, favourable velocities exist on the side of the river without a fishway entrance (albeit in a turbulent region). The flow velocities in all remaining scenarios are too high for glass eel to successfully reach the fishway. For salmon, the velocities are generally favourable, and only the highest discharge scenario (330 m³/s through the weir closest to the fishway) features some areas of burst velocities. All in all, this means that none of the scenarios resulted in a straightforward combination of both passable turbulence and the right flow velocities. It was shown that applying different weir gate configurations that achieve that same discharge result in significantly different migration routes. This highlights the importance of weir configuration and weir type (i.e., having few large versus many small gates over the width of the river). This also means that this set of scenarios is not exhaustive: weir configurations might exist for which these discharges can result in (more) favourable flow patterns.

Samenvatting [NL]

Voor het ontwerp van een effectieve vistrap zijn kennis van visgedrag en waterbouwkunde even belangrijk. Veel natte kunstwerken in Nederland zijn aan het verouderen en zullen in de komende decennia vervangen worden. Dit betekent dat er veel nieuwe kunstwerken ontworpen zullen gaan worden. Het is belangrijk dat ecologen en waterbouwkundigen samenwerken om in de toekomst tot een voor migrerende vis succesvol stuw- en vistrap ontwerp te komen. Vanzelfsprekend is observeren in het veld de gouden standaard voor ecologisch onderzoek naar visgedrag, maar voor natte kunstwerken die nog niet gebouwd zijn is een andere methode nodig om de effectiviteit van vistrappen te beoordelen. Dit rapport demonstreert de inzetbaarheid van Computational Fluid Dynamics (CFD) om in deze behoefte te voorzien aan de hand van stuw Grave als casus.

Door de eisen van vissen te kwantificeren voor een groep doelsoorten, kunnen kunstwerken al bij ontwerp geoptimaliseerd worden voor vismigratie. Dit is een verbetering ten opzichte van het verleden: vaak werden oplossingen voor vismigratie achteraf toegevoegd, zoals bij de stuwen in de Maas. De effectiviteit van een vistrap bestaat uit meerdere aspecten: de vindbaarheid, bereikbaarheid, passeerbaarheid en totale benodigde tijd. De vindbaarheid is hierbij de eerste essentiële stap, een vistrap die niet gevonden kan worden kan immers zeker niet gepasseerd worden. De focus van deze casus ligt daarom bij de vindbaarheid van de vistrap bij stuw Grave.

Er zijn twee concepten beschouwd: de migratielimietslijn en het continue migratiepad. De migratielimietslijn bakent een gebied af waarin de stroomsnelheden en turbulentie te sterk zijn om tegen op te zwemmen. Het continue migratiepad beschrijft het gebied waarin de snelheden niet te laag maar ook niet te hoog zijn, en waarin de turbulentie voldoende laag is. De limieten aan de zwemprestaties van verschillende vissoorten zijn beschikbaar in literatuur van veld- en labproeven. De CFD simulaties zijn in dit rapport geïnterpreteerd aan de hand van de capaciteiten van glasaal en zalm. Turbulentie wordt in de literatuur vaak genoemd als een van de belangrijkste stromingseigenschappen, maar de limieten worden zelden gekwantificeerd en zijn ook niet specifiek per vissoort.

CFD is met succes toegepast om de gevolgen van stuwbeheer voor vismigratie te bepalen. Op basis van de uitgevoerde CFD simulaties kan worden geconcludeerd dat de vistrap bij stuw Grave niet voldoende vindbaar lijkt om grootschalige migratie mogelijk te maken. De vistrapingang is in bijna alle simulaties verborgen achter een gebied met te sterke turbulentie. Het enige scenario met voldoende lage turbulentie ($100 \text{ m}^3/\text{s}$ door de grote stuw) bracht andere uitdagingen met zich mee: er ontstonden te lage (niet-aantrekkelijke) snelheden voor de vistrap. Voor de glasaal, die graag bij de bodem leeft, is er in dat scenario alleen een pad beschikbaar dat erg dicht bij het wateroppervlak zit. Voor de zalm zijn er in dat scenario aantrekkelijkere snelheden aan de verkeerde kant van de rivier. In alle andere scenario's zijn de stroomsnelheden te hoog voor glasaal. Voor zalm zijn de stroomsnelheden over het algemeen acceptabel, alleen in het hoogste scenario ($330 \text{ m}^3/\text{s}$ door de kleine stuw) bestaat een deel van de stroming uit de sprintsnelheid. Al met al was in geen van de scenario's sprake van een eenduidige combinatie tussen de juiste snelheden en turbulentieniveaus. Uit simulaties met verschillende schuivenconfiguraties, die steeds in een andere configuratie dezelfde totale afvoer veroorzaken, blijkt dat het stuwbeheer een grote invloed heeft op de migratiepaden die ontstaan. Dit geeft het belang van visvriendelijk stuwbeheer weer, en betekent ook dat nog niet alle opties uitgeput zijn: er zouden stuwconfiguraties mogelijk kunnen zijn waardoor de beschouwde afvoeren tot gunstigere stroming kunnen leiden.

Content

	Summary [EN]	4
	Samenvatting [NL]	5
	Content	6
1	Introduction	8
1.1	Study site: Weir Grave	9
1.2	Report outline	10
2	Fishway findability	11
2.1	Attraction flow	11
2.1.1	Discharge ratio	12
2.1.2	Location	12
2.1.3	Flow angle	12
2.2	Migration limit line	13
2.2.1	Flow velocity	13
2.2.2	Flow turbulence	14
2.2.2.1	Turbulent kinetic energy	15
2.2.2.2	Vorticity	15
2.3	Fish-friendly weir operation	16
3	Numerical modelling set-up and validation	17
3.1	CAD model and bathymetry	17
3.2	Boundary conditions	18
3.3	Computational mesh	20
3.4	Validation based on field measurements	21
3.4.1	Conditions in the field	22
3.4.2	Velocity fields in the main river section	23
3.4.3	Velocity field in the fishway outflow	26
4	Results	28
4.1	Discharge ratio	28
4.2	Velocity	29
4.2.1	European eel	29
4.2.2	Atlantic salmon	32
4.3	Turbulence	36
4.3.1	Turbulent kinetic energy	36
4.3.2	Vorticity	40
5	Conclusion	42
5.1	Recommendations for further research	43

1 Introduction

Fish migration forms an essential part of freshwater ecosystem health. Migratory fish populations worldwide have, however, declined by 81% since 1970 (Deinet et al., 2024). The construction of weirs in our rivers contributes to this decline by disconnecting waterbodies and fish migration routes. To mitigate this effect, all weirs in the river Meuse were equipped with fishways, typically located inside concrete pillars or abutments. These fishways did not work properly, have since been shut down, and were replaced by nature-like bypass fishways (Rijkswaterstaat, 2023a). Unfortunately, also the nature-like fishways do not perform optimally (ATKB, 2021).

Hydraulic structures are often viewed as obstacles solely due to the resulting head difference. Whether a structure can be found and passed or not, however, greatly depends on the hydrodynamic conditions just downstream of a structure and how these compare to the swimming performance and leaping capabilities of the native fish species (Larinier, 2002). The overall effectiveness of a fishway consists of multiple aspects (also see Figure 1.1):

- Findability: what percentage of fish can find the fishway?
- Accessibility: what percentage of fish can enter the fishway?
- Passability: what percentage of fish can pass the entire fishway?
- Time: how much delay is caused by finding, entering and passing the fishway?

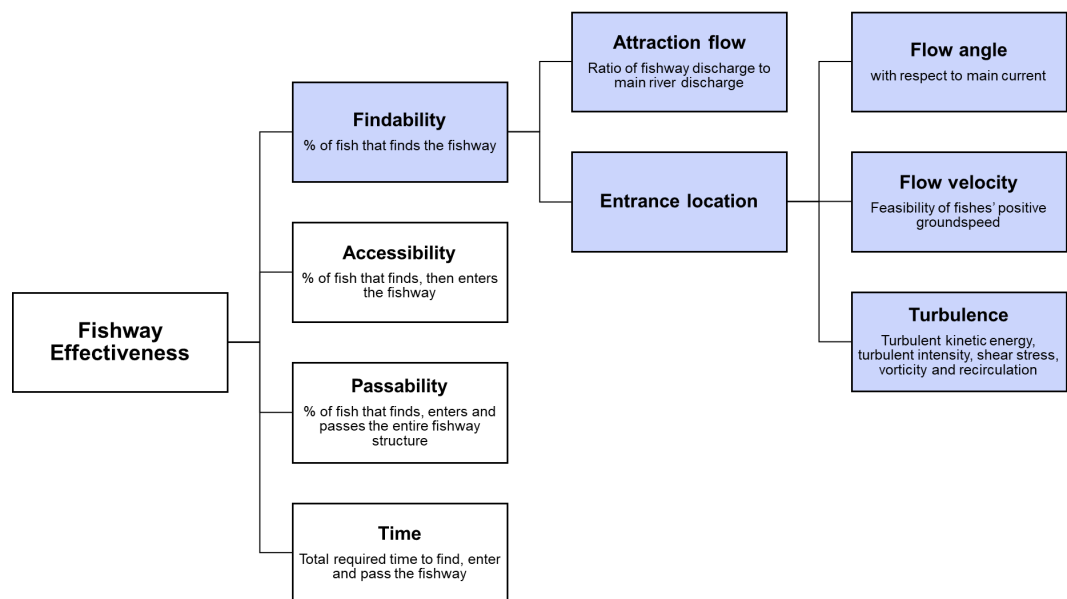


Figure 1.1: [EN] The four dimensions of fishway effectiveness: findability, accessibility, passability and total time spent. The scope of the present study, the different aspects of findability, is shaded in blue. [NL] De vier dimensies van de vispassage effectiviteit: vindbaarheid, bereikbaarheid, passeerbaarheid en de totale benodigde tijd. De focus van deze studie, de verschillende aspecten van vindbaarheid, is blauw gearceerd.

The findability of the entrance of a fishway is an essential component of a fishway's total effectiveness, considering that a fishway that cannot be found, cannot be passed. Designing effective fishways requires both ecological knowledge of fish behaviour in highly variable flows, and hydraulic engineering knowledge to create favourable hydraulic conditions for fish (Williams et al., 2011). The hydraulic conditions near the fishway should be such that fish are attracted or guided to the entrance, which should not be hidden behind recirculation zones, stagnant water or turbulent flow originating from the weir (Larinier, 2002).

Developing knowledge on the effectiveness of the fishways in the river Meuse is important for biodiversity and particularly pressing given the legal obligation to fulfil the European Water Framework Directive's (WFD) goals (KRW, 2000). Internationally, Computational Fluid Dynamics (CFD) is frequently utilised in the assessment and design of fish guiding structures, including fishways, that should be passable by fish (Redeker & Heimerl, 2018; Gisen et al., 2017; Li & Zheng, 2009; Daneshvar et al., 2017; Flores et al., 2022). Van Daal-Rombouts et al. (2014) have shown that CFD models can accurately reproduce the hydraulic behaviour of complex hydraulic structures by comparison to a physical scale model of an overflow weir.

The weirs in the Meuse are aging and will need to be renovated, replaced, or otherwise renewed in the coming decades (Rijkswaterstaat, 2022b). It is important for ecologists and engineers to work together to achieve hydraulic conditions that allow for successful fish migration (Williams et al., 2011) and thereby meet WFD goals. The field of ecology is understandably heavily based on observing the natural world (Sagarin & Pauchard, 2012), but the future weirs (in the design phase) cannot be observed in the field yet. There may also be cases where the situation in the field may be difficult to observe (hard to reach). Hence, another way to reliably predict whether fish will be able to pass such structures must be found. To demonstrate the applicability of CFD for this purpose, the present study applies 3D CFD to quantify the findability of the entrance of the fishway at weir Grave.

1.1 Study site: Weir Grave

The analysis of the findability of fishways is applied to lock- and weir complex Grave (51° 46' 9" N, 5° 44' 12" E) in the river Meuse. The entire complex consists of a weir, two navigation locks (one non-operational) and a fishway (see Figure 1.2). The navigation locks are not part of the studied and modelled area.

Weir Grave consists of two reverse Poirée weirs connected to a road traffic bridge (see Figure 1.2). The Poirée weirs consist of twenty supports and sixty gates (across three rows) that can be moved as pairs and individually, respectively. Removing a gate from the top two rows increases the discharge by approximately 25 m³/s, while removing a gate from the bottom row results in 12 m³/s additional discharge (Rijkswaterstaat, 2023b). Once all gates have been removed, the supports can be flipped up towards the bridge, allowing the Meuse to flow freely.



Figure 1.2: **[EN]** Lock- and weir complex Grave in the river Meuse. **[NL]** Sluis- en stuwcomplex Grave in de Maas. © Rijkswaterstaat | Joop van Houdt.

The fishway at weir Grave (see Figure 1.3 and Figure 1.4) is a 470 metres long nature-like bypass that consists of sixteen sills and a control structure at the upstream end. The control structure is controlled automatically based on the water level upstream of weir Grave. The other sills are V-shaped and have two vertical slots, one in the middle and one on an alternating side. The head difference over each sill is approximately twenty centimetres. The fishway was designed to work optimally at the maximum head difference (three metres) that occurs at the weir (ATKB, 2021). The discharge through the fishway is approximately 4 m³/s, but research by ATKB (2021) has shown that the control structure at the upstream most sill was often set incorrectly in practice, resulting in discharges that were too low in the fishway. ATKB (2021) also found that high river discharges can result in complete submersion of the sills at the downstream end, resulting in insufficient attraction flow.

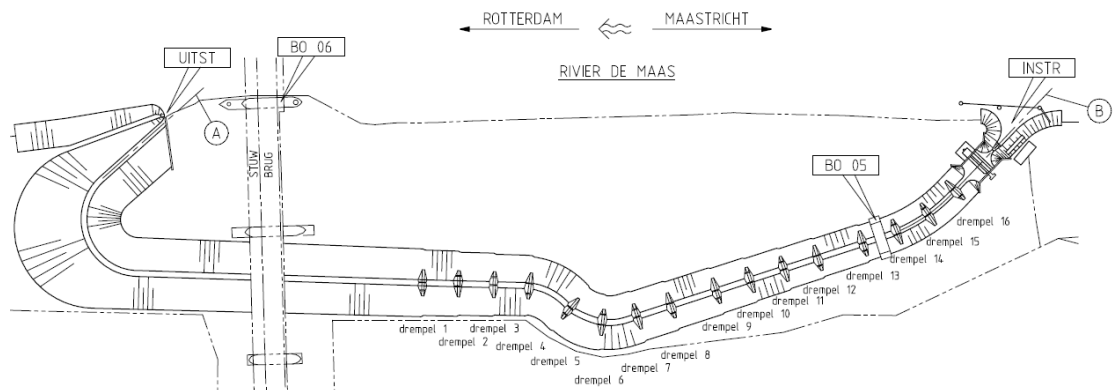


Figure 1.3: [EN] Top view of the fishway at lock- and weir complex Grave (Rijkswaterstaat, 2011). [NL] Bovenaanzicht van de vistrap bij stuw- en sluiscomplex Grave (Rijkswaterstaat, 2011).

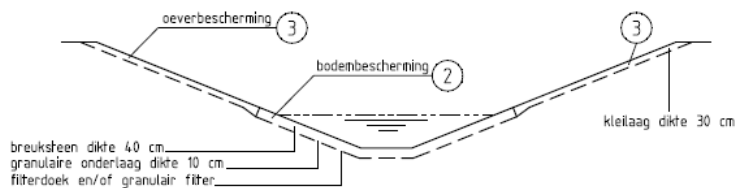


Figure 1.4: [EN] Cross-section of the fishway sections in-between the sills (Rijkswaterstaat, 2011). [NL] Dwarsdoorsnede van de secties van de vistrap tussen de drempels (Rijkswaterstaat, 2011).

1.2 Report outline

This report is structured as follows: Chapter 2 describes the findings of literature research on the topic of fishway findability and fish-friendly weir operation. Chapter 3 describes the set-up of the numerical models and the field measurement campaign that was conducted at weir Grave to validate the model. Chapter 4 presents the results of the simulation and finally, Chapter 5 consists of conclusions and recommendations for further research. All figure captions include a Dutch translation, marked by [NL].

2 Fishway findability

Fish use their lateral line system to sense flow velocities and pressure differences in their environment. These pieces of hydrodynamic information then form the basis of their behavioural decision-making (Bleckmann & Zelick, 2009). Kroes & Monden (2005) summarise the behaviour of fish near hydraulic structures as follows: Fish will...

- approach the hydraulic structure along the riverbank with the strongest flow;
- assemble close to the structure at their *migration limit line*;
- search for an alternative route in the upstream direction (highlighted by *attraction flow*) along their migration limit line, where they might cross the length of the migration limit line multiple times per day;
- seek shelter close to riverbanks.

This chapter summarises the findings of literature research performed to understand fish behaviour near hydraulic structures and the different aspects of fishway findability. The following sections will elaborate on the concepts of attraction flow (Section 2.1) and the migration limit line (Section 2.2), specifically targeted at weirs with nature-like bypass fishways (see Figure 2.1). These sections will mainly address the roles of flow velocity and turbulence. Temperature, aeration, light and noise levels also influence fishway findability (Brandl et al., 2022), but will not be considered further in the present study. Finally, Section 2.3 discusses the role of (fish-friendly) weir operation in fishway findability.



Figure 2.1: **[EN]** Example of a migration limit line location near the fishway entrance and direction of the attraction flow at weir Grave (photo adapted from Rijkswaterstaat (2023a)). **[NL]** Voorbeeld van de locatie van de migratielimietlijn en de richting van de lokstroom bij de ingang van de vistrap van stuw Grave (foto bewerkt uit Rijkswaterstaat (2023a)).

2.1 Attraction flow

Because fish orientate themselves by the direction of the flow, fishways have a discharge with the function of making fish aware of the fishway's presence. This discharge is referred to as

attraction flow. If several flow 'paths' with different velocities overlap, fish will follow the current with the highest (yet conquerable, see Section 2.2.1) velocity (Larinier, 2002). The attraction flow therefore needs to be distinguishable from the main flow, without obstruction caused by strong turbulence, reverse flow or stagnating flow. The successfulness of the realised attraction flow depends on three factors:

1. The magnitude of the discharge with respect to the discharge in the main waterway (Section 2.1.1)
2. The location with respect to the hydraulic structure (Section 2.1.2)
3. The angle of the attraction flow with respect to the direction of the main flow (Section 2.1.3)

2.1.1 Discharge ratio

Overall, fishway findability can be improved by maximising the magnitude of the attraction flow (Coenen et al., 2013). There are no exact criteria for the minimum ratio between fishway discharge and main river discharge. Larinier (2002) suggested a widely accepted attraction flow magnitude of approximately 1–5% of the main discharge, but subsequently acknowledges that an incorrect entrance position (see Section 2.1.2) might result in a higher discharge requirement. In France, the UK and the USA, the magnitude of fishway attraction flows is typically 5 – 10% of the total discharge at the hydraulic structure (Williams et al., 2011). The chosen design discharge in the design of a fishway should at least be equal to the lowest discharge that can occur during the migratory season (Coenen et al., 2013).

The magnitude of the fishway discharge at weir Grave could therefore be a shortcoming. The fishway discharge is never larger than 4 m³/s (and equal to approximately 3.5 m³/s in practice, see Section 3.4). This means that whenever the discharges are greater than 400 m³/s, per Larinier's (2002) minimum criterion of 1 – 5%, more than the maximum of 4 m³/s of attraction flow would be required. The consequences of this potential shortcoming is fish species specific, as discharges of this magnitude are most likely to occur in specific seasons, which then may or may not overlap with their unique migration period.

2.1.2 Location

The location of the entrance to the fishway is crucial to fishway effectiveness as fish cannot pass a fishway that they cannot find. Areas that are unattractive to fish, for example far away from the hydraulic structure where flow velocities are low, must be avoided as fish will instead follow the main flow of the river. Because of this, most successful fishways have their entrance as close to the hydraulic structure as possible (Williams et al., 2011). However, areas too close to a hydraulic structure should be avoided since high turbulence could obstruct the fishway entrance.

Fishways placed in the middle of a hydraulic structure do not attract fish very effectively because fish tend to approach hydraulic structures along the riverbanks (Williams et al., 2011). This may be one of the contributing factors to the ineffectiveness of the fishways that had initially been built in the pillars of the weirs in the Meuse.

2.1.3 Flow angle

During high river discharge, a perpendicular jet would be broken up quickly and would not persist far downstream (Larinier, 2002). Attraction flows perpendicular to the main river flow have therefore been found to work poorly (Williams et al., 2011). Instead, the flow should be almost parallel to, or at a slight angle (< 30°) with respect to the main flow (Pavlov, 1989), so that fish can swim into the attraction current as directly as possible (Williams et al., 2011). During low river discharge, however, it can be beneficial to angle the fishway entrance perpendicularly to the main flow to maximise the reach of the attraction flow (Larinier, 2002). A theoretical shortcoming of the Grave fishway is therefore the angle of the attraction flow.

The entrance is angled such that the attraction flow is perpendicular to the main flow (Rijkswaterstaat, 2023b). The (stronger) main flow will quickly break up the fishway's jet, causing the attraction flow to become imperceptible.

2.2 Migration limit line

Migrating fish will generally follow the strongest flow until they reach the limit of their swimming performance. The location of this limit is referred to as the 'migration limit line' and is typically characterised by very high flow velocity (see Section 2.2.1) and/or turbulence (see Section 2.2.2). As fish reach this limit, they will start searching for an opportunity to continue their path upstream along the migration limit line (WL | Delft Hydraulics, 2006). Contrary to what the name migration limit *line* implies, this velocity/turbulence barrier is a three-dimensional surface within the water column.

Ideally, the entrance of the fishway is located at a point where the migration limit line reaches the riverbank (see Figure 2.1). Fishway entrances in the river Meuse do not have control structures and are therefore always located in the same position. The location of the migration limit line, on the other hand, can vary significantly. This variation is caused by the characteristics of the flow (and therefore the configuration of the weir) but is also specific to the swimming performance of fish. This means that every combination of a weir configuration (with its corresponding flow velocities and turbulence levels) and fish species (during a specific life stage) has its own unique migration limit line.

2.2.1 Flow velocity

The ideal flow velocity in the vicinity of the fishway entrance is bounded by the swimming performance of the weakest fish and the lowest perceptible (rheoactive) velocity (Brandl et al., 2022). To successfully reach the fishway, the fish must have a positive groundspeed, meaning that their swimming speed needs to be greater than the flow velocity. The energy required is however also dependent on flow variations or turbulence, see Section 2.2.2.

Figure 2.2 shows how the swimming performance of fish depends on for how long a certain speed needs to be maintained. The prolonged (maintained for 20 seconds to 200 minutes; (Wolter & Arlinghaus, 2004)) and sustained (maintained for >200 minutes; (Wolter & Arlinghaus, 2004)) swimming speeds are considered as the feasible speeds during upstream migration in this study. A continuous migration corridor is an area in the flow field where using sustained and prolonged swimming speeds would suffice. The burst (<20 seconds; (Wolter & Arlinghaus, 2004)) swimming speed that can only be maintained for a few seconds is considered as the start of the migration limit line.

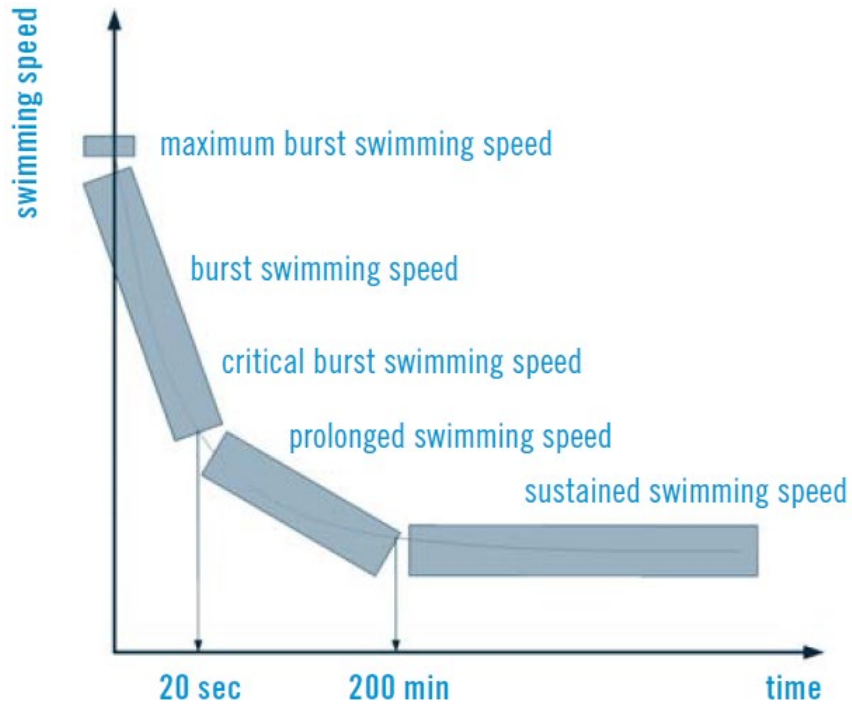


Figure 2.2: [EN] The categories of swimming performance of fish as a function of time (ICPDR, 2013). [NL] De verschillende categorieën zwemprestaties van vissen als functie van tijd (ICPDR, 2013).

The fish species that were studied are the juvenile European eel (*Anguilla anguilla*) and adult Atlantic salmon (*Salmo salar*). Some general characteristics, as well as the rheoactive, sustained, prolonged and burst velocities for both of these fish species are listed in Table 2.1. The sustained velocities are not mentioned explicitly in literature, and have instead been derived from the range between the rheoactive velocity (ICPDR, 2013) and the lower sustained velocity (Winter et al., 2014).

Table 2.1: General characteristics and swimming capacity of the studied fish species.

Characteristics	European eel (<i>Anguilla anguilla</i>)	Atlantic salmon (<i>Salmo salar</i>)
Migration guild	Catadromous	Anadromous
Flow preference	Eurytopic	Rheophilic
Upstream migration period	Feb – June	May – Dec
Upstream migration life stage	Juvenile	Adult
IUCN Red List Status (IUCN, 2024)	Critically Endangered	Near Threatened
Rheoactive velocity (ICPDR, 2013)	0.15 m/s	0.15 m/s
Sustained velocity	0.15 – 0.2 m/s	0.15 – 0.6 m/s
Prolonged Velocity (Winter et al., 2014)	0.2 – 0.3 m/s	0.6 – 0.9 m/s
Burst velocity (Winter et al., 2014)	0.3 – 0.5 m/s	2.0 – 10.0 m/s

2.2.2 Flow turbulence

The degree to which fish are hindered by turbulence depends on characteristics such as body length and swimming capacities, but relatively little is known about the (quantified) turbulence limit of fish (Arcadis, 2018). Fish exert more energy in highly turbulent flows and their swimming performance is diminished compared to laminar flow (Marriner et al., 2014). Fish must be able to stabilize their posture and swimming trajectory (Cotel & Webb, 2015). Additionally, research

has shown that the disorientation that is caused by turbulence results in a reduced response to predation (Odeh et al., 2002).

There are multiple ways¹ to characterise turbulence. In the present study, the turbulence levels will be evaluated based on turbulent kinetic energy (Section 2.2.2.1) and vorticity (Section 2.2.2.2).

2.2.2.1 Turbulent kinetic energy

The turbulent kinetic energy k , is defined as

$$k = \frac{1}{2} (\overline{u'^2} + \overline{v'^2} + \overline{w'^2}), \quad (2.1)$$

with u' , v' and w' the fluctuating components of the velocities in the x -, y - and z -direction, respectively. Turbulent kinetic energy can be viewed as a measure for the intensity of turbulent flow. In general, for all fish species, the migration limit is $k = 0.05 \text{ m}^2/\text{s}^2$, where $k \leq 0.05 \text{ m}^2/\text{s}^2$ is considered 'low', and $k > 0.05 \text{ m}^2/\text{s}^2$ is considered 'high' (Marriner et al., 2014).

2.2.2.2 Vorticity

The lateral line system allows fish to perceive the vortices generated by movements around them, like for example the movements of other organisms, or the wake of hydraulic structures (Muhawenimana et al., 2019). Overall, rapidly rotating vortices, particularly with a diameter roughly equal to (Tritico & Cotel, 2010), or greater than (Marriner et al., 2014) a fish's body length, can lead to disorientation and difficulty maintaining a stable posture. In lab experiments, loss of postural control occurred more than twice as often due to vortices in the horizontal plane than in the vertical plane (Tritico & Cotel, 2010). However, a more recent study comparing hydrodynamic forces of similar magnitudes by Muhawenimana et al. (2019) found that negative (clockwise) vorticity in the vertical plane could be particularly detrimental for swimming stability.

The vorticity in the horizontal plane ω_z , or the rotation around a vertical axis in the z -direction, is defined as:

$$\omega_z = \left(\frac{\partial v}{\partial x} - \frac{\partial u}{\partial y} \right). \quad (2.2)$$

with u and v the velocities in the x - and y -direction. For vorticity, the migration limit is $\omega_z = 3.0 \text{ s}^{-1}$, where $\omega_z \leq 3.0 \text{ s}^{-1}$ is considered 'low', and $\omega_z > 3.0 \text{ s}^{-1}$ is considered 'high' (Marriner, et al., 2014). The entrance of a fishway should not be masked by a recirculation zone (Pavlov, 1989).

Vorticity in the vertical plane ω_y , is defined as:

$$\omega_y = - \left(\frac{\partial u}{\partial z} - \frac{\partial w}{\partial x} \right). \quad (2.3)$$

with w the velocity in the z -direction. Muhawenimana et al. (2019) emphasised the importance of the direction of hydrodynamic forces in the interpretation of its effect on fish.

¹ Silva et al. (2012) have identified Reynolds' shear stress as one of the most important turbulent flow parameters for fish. The forces that are generated (parallel on a fish's body) have a significant influence on a fish's swimming ability and stability, and in extreme cases can even cause physical harm (Odeh, et al., 2002). The present study applies a two-equation turbulence model approach (see Section 3.2) and therefore cannot resolve the six unknowns of the Reynolds' stress tensor.

2.3 Fish-friendly weir operation

The river Meuse is fed by rain and has a relatively small catchment area, which can cause large fluctuations in the discharge. The lowest and highest discharges measured at monitoring station St. Pieter, which is the closest monitoring station to the Meuse's entrance into The Netherlands, are approximately 30 m³/s en 3000 m³/s, respectively (Rijkswaterstaat, 2023a; Platform Rivierkennis, 2018). Due to this large range of discharges and the differences in migratory behaviour of the various fish species that belong in the river Meuse, picking the ideal entrance location is not straightforward. In such cases, fishway efficiency could be improved by creating multiple entrances (Larinier, 2002).

Despite the single fishway entrance at the weirs in the Meuse, 'fish-friendly' weir operation could ensure that the migration limit line is in the right location during the migration season. Measurements of the flow velocities at the Sambeek weir have shown that it was possible to control the flow velocities such that the conditions near the fishway were suitable for migratory fish (WL | Delft Hydraulics, 2006). The same study also assessed the ease of implementation and found fish-friendly weir operation to be easy to implement by the weir operators, but its effectiveness could not be determined because ultimately only two of the fifty-two tagged fish passed the fishway.

Figure 2.3 shows a few examples of fish- (un)friendly weir operation. Note that in Figure 2.3, contrary to the weirs in the Meuse, the fishways are located on both sides of the river. For the weir construction it is generally preferable to distribute the discharge evenly over the entire weir to ensure that the stilling basin and bed protection wear evenly. For fish, you might want to concentrate the discharge at a specific location, for example in the low discharge example in Figure 2.3b. It would therefore be good to take fish-friendly weir operation into account in the design of the new weirs in the Meuse.

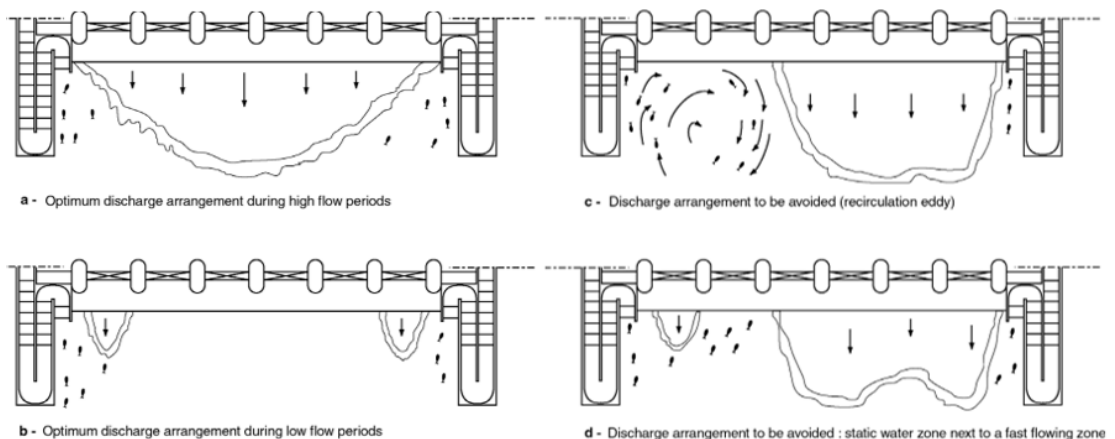

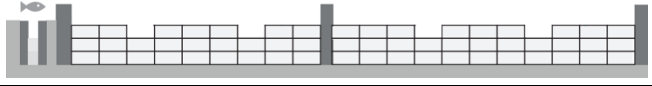
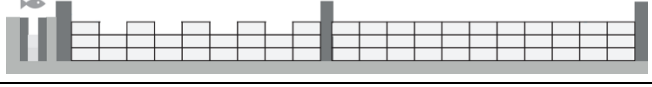
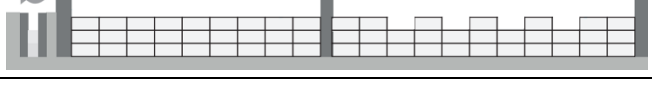



Figure 2.3: **[EN]** Two examples of optimal discharge distributions at high (a) and low discharge (b), and distributions to avoid due to recirculation (c) or zones of stagnant water (d) (Larinier, 2002). **[NL]** Twee voorbeelden van ideale verdelingen van hoge (a) en lage afvoer (b), en verdelingen die vermeden moeten worden vanwege recirculatie (c) of gebieden met stilstaand water (d).

3 Numerical modelling set-up and validation

CFD software package Simcenter STAR-CCM+ 2021.2 Build 16.04.007 was used for all simulations. STAR-CCM+ is a commercially available multi-physics software package that includes several meshing algorithms, different types of boundary conditions, numerical schemes and turbulence models. Simulations were performed for five different conditions, each with a unique weir gate configuration. Table 3.1 shows the weir gate configuration and corresponding approximate discharge for each simulation. From the simulation with $Q \approx 250 \text{ m}^3/\text{s}$ it became apparent that the flow near the fishway entrance was very turbulent. Based on this observation, the choice was made to focus on a smaller discharge of $Q \approx 100 \text{ m}^3/\text{s}$, but achieved through different weir gate configurations. The numerical simulations in this study have been carried out at full scale.

Table 3.1: Simulated discharges and the corresponding weir gate configurations.

Simulation	Discharge	Weir gate configuration
S250	$Q \approx 250 \text{ m}^3/\text{s}$	
S100	$Q \approx 100 \text{ m}^3/\text{s}$	
S100-L	$Q \approx 100 \text{ m}^3/\text{s}$	
S100-R	$Q \approx 100 \text{ m}^3/\text{s}$	
S330	$Q \approx 330 \text{ m}^3/\text{s}$	

This chapter describes the numerical set-up of the CFD model. Section 3.1 describes the 3D Computer Aided Design (CAD) model of the weir Grave, the fishway and the bathymetry up- and downstream of the weir. Sections 3.2 and 3.3 describe the imposed boundary conditions and the computational mesh, respectively. Additionally, Rijkswaterstaat performed field measurements in the fishway and in the main river section up- and downstream of the weir. These measurements were used to validate the CFD model (simulation S330 in Table 3.1). Section 3.4 shows the results of the validation study.

3.1 CAD model and bathymetry

Figure 3.1 shows the CAD model of weir Grave. Each of the gates (red, white and blue) and each pair of supports (green) can be moved to recreate the configurations as they occur in the field. The bathymetry in the stretch of the Meuse around weir Grave is shown in Figure 3.2. The exact bathymetry in the fishway is not known to the same detailed extent. The connection between the fishway and riverbed is quite uncertain as a result and may contain sharper angles than exist in practice. The CAD drawing of the fishway is therefore based solely on Figure 1.3 and Figure 1.4.

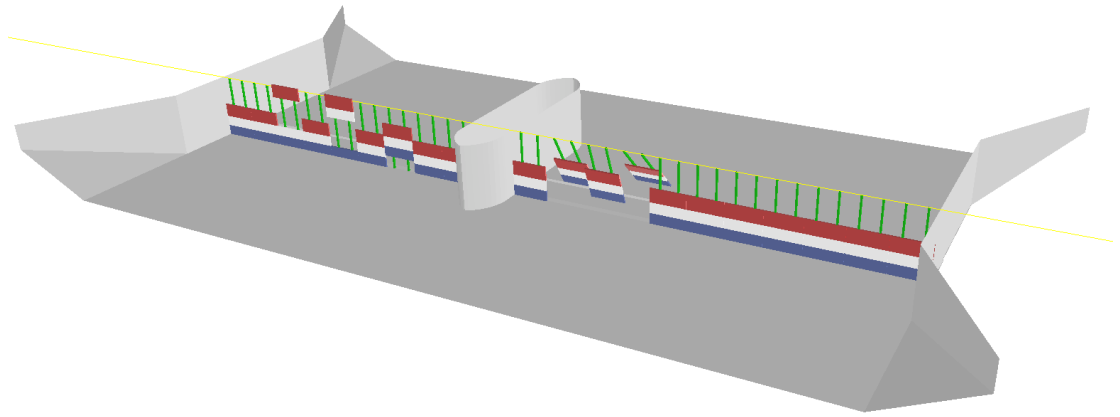


Figure 3.1: **[EN]** Computer Aided Design (CAD) model of the weir Grave with adjustable gates and supports. **[NL]** Computer Aided Design (CAD) model van stuw Grave, met beweegbare schuiven en jukken.

Simcenter STAR-CCM+

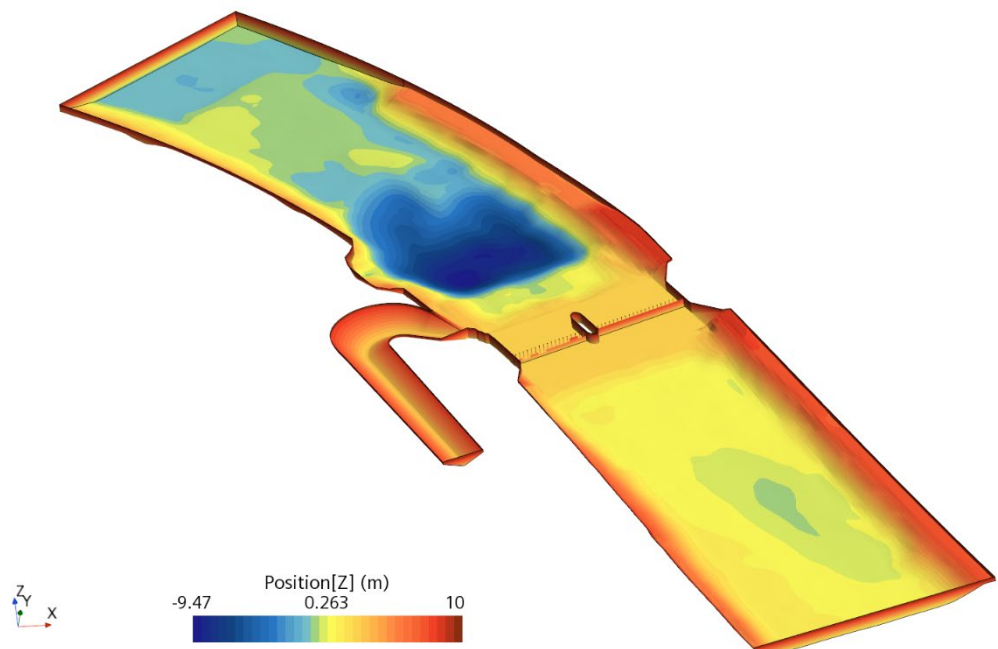


Figure 3.2: **[EN]** Bathymetry surrounding the weir Grave in metres with respect to NAP. **[NL]** Bathymetrie in de directe omgeving van stuw Grave in meters ten opzichte van NAP.

3.2 Boundary conditions

The flow equations (continuity and momentum) are modelled using the Unsteady Reynolds-Averaged Navier-Stokes (URANS) approach. This approach leads to a prediction of the mean flow velocities. The effect of turbulence on the mean flow is modelled using turbulence transport equations, which give a prediction of the location and strength of turbulence, using these to adjust the mean flow. Fluctuating turbulent velocities are therefore unavailable from the output of this model. Other turbulence models do give predictions of the fluctuating velocities but are much more computationally expensive. The specific turbulence model that was used in these simulations is the realisable $k - \varepsilon$ model (Launder & Spalding, 1974), which is the most widely used turbulence model and the recommended model for STAR-CCM+ (Siemens, 2021). When using a turbulence model, the physics of the turbulent boundary layers, such as those near the riverbed and structures, must be modelled explicitly.

The Volume of Fluid (VOF) model was applied to model air and water as immiscible phases. The height of the free surface was enforced at +7.90 m NAP and +4.90 m NAP at the in- and outlet, respectively, as these are the target water levels for the weir operators. These water levels are only enforced at the boundary cell, the water level in the regions in-between is calculated by the model. The local water levels and the discharges depend on the resistance caused by the configuration of the weir gates. The downstream boundary wraps around the corner of the numerical domain until it reaches the longitudinal dam (see Figure 1.2) between the main waterway and the navigation lock. The no-slip condition is imposed on all walls in the numerical domain. An overview of the boundary conditions is shown in Figure 3.3.

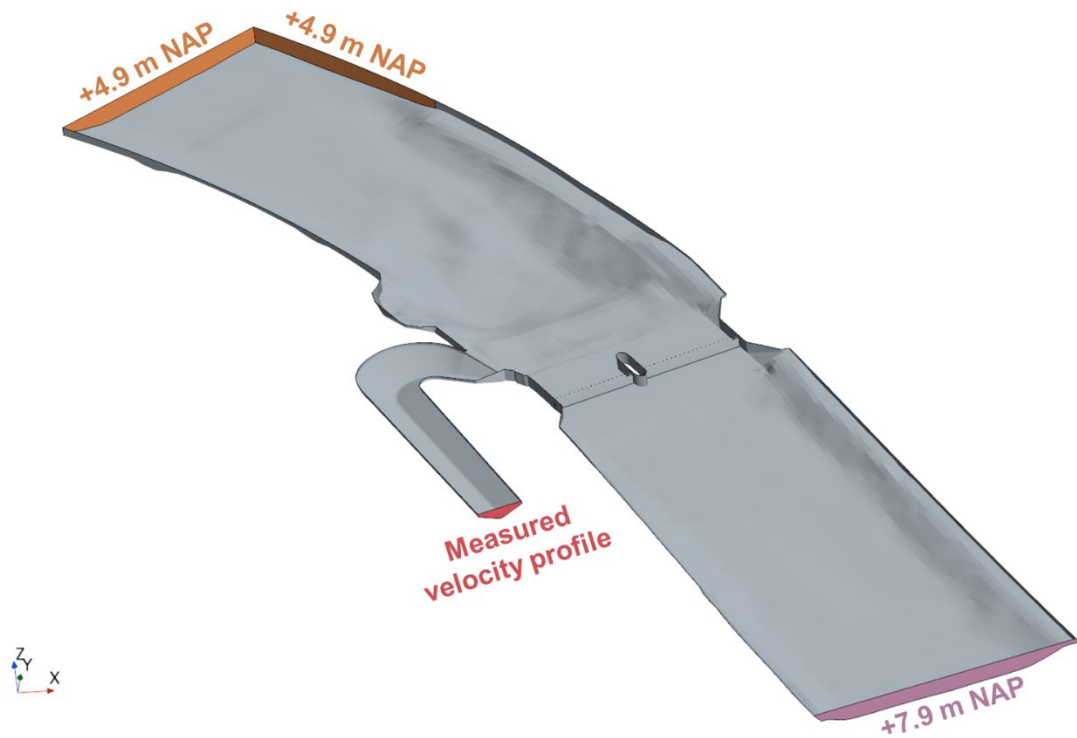


Figure 3.3: **[EN]** Overview of the imposed boundary conditions. The up- (purple) and downstream (orange) boundaries impose a certain water level at the very edge of the numerical domain. The fishway inlet boundary imposes a measured velocity profile (red, see Figure 3.4). The no-slip condition is applied to all walls (grey). **[NL]** Overzicht van de opgelegde randvoorwaarden. De boven- (paars) en benedenstroomse (oranje) randen specificeren het waterniveau op de rand van het domein. De rand in de inlaat van de vistrap (rood) legt een gemeten snelheidsprofiel op (zie ook Figure 3.4). Op alle overige randen (grijs) geldt de no-slip voorwaarde.

In addition to validation, the field measurement campaign (see Section 3.4) also provided velocity profiles for the upstream boundary of the fishway (red in Figure 3.3). The imposed velocity profile, based on the average of twelve measured profiles at that location, is shown in Figure 3.4. The performed Acoustic Doppler Current Profiler (ADCP) measurements do not capture the top twenty centimetres of the water column (between +4.8 and +5.0 m NAP in Figure 3.4). The velocities measured at +4.8 m NAP were therefore assumed to also be representative for the top layer. Despite not knowing the exact bathymetry and water levels in the fishway (see Section 3.1), this measured profile has ensured that the velocity and discharge through the fishway are representative of the field conditions. The discharge through the fishway at the time of the field measurements was approximately 3.5 m³/s, which is equal to the discharge that was realised in the CFD simulations by imposing the measured velocity profile.

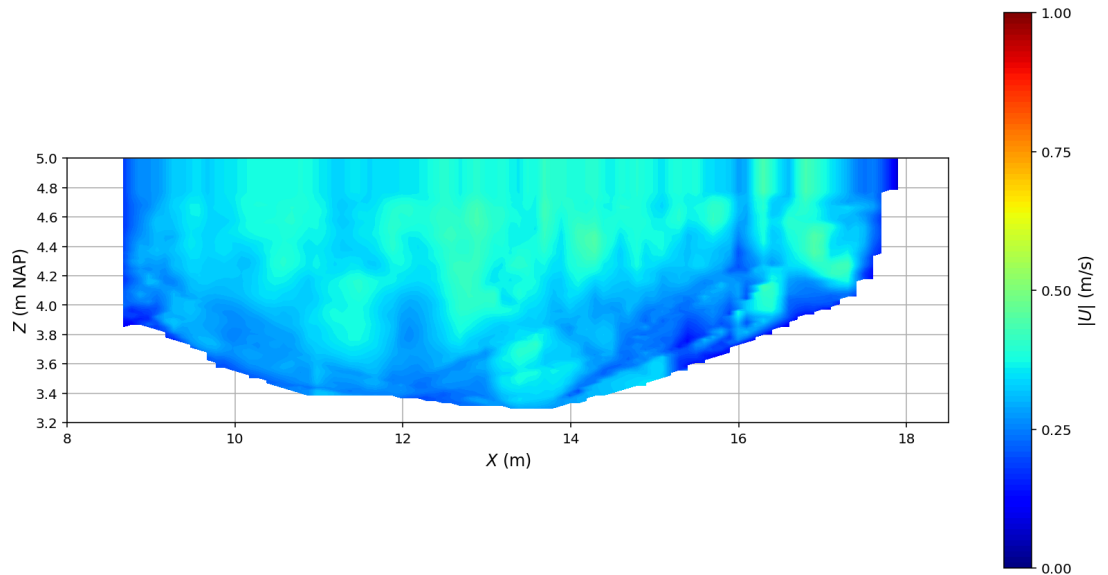


Figure 3.4: **[EN]** Average velocity magnitude of twelve velocity profiles measured just downstream of the final sill. **[NL]** Stroomsnelheid gemiddeld over 12 gemeten snelheidsprofielen net benedenstrooms van de meest benedenstroomse drempel in de vistrap.

3.3 Computational mesh

The computational mesh was generated using the STAR-CCM+ trimmer mesh algorithm, which results in predominantly square cells, with prismatic shapes near boundaries and where necessary a so-called prism layer to capture the velocity gradients near solid boundaries.

A grid refinement study based on the concept of Richardson extrapolation was carried out to assess the mesh quality (NASA, 2021). Richardson extrapolation allows you to obtain a higher-order estimate of the continuum value from a series of lower-order discrete values (Roache, 1994). As the grid resolution approaches zero, the results should start approaching the 'real' value.

Three grids (base sizes 100, 75 and 50 cm) were analysed. The results of Richardson extrapolation for the quantities of interest velocity magnitude, turbulent kinetic energy and discharge are shown in Figure 3.5. The calculated order of convergence results in an error of 0.97%, 47.9% and 0.90% for velocity magnitude, turbulent kinetic energy and discharge, respectively. This indicates good convergence for velocity magnitude and discharge, but less so for turbulent kinetic energy, which is known to be difficult to predict (Zubova et al., 2022).

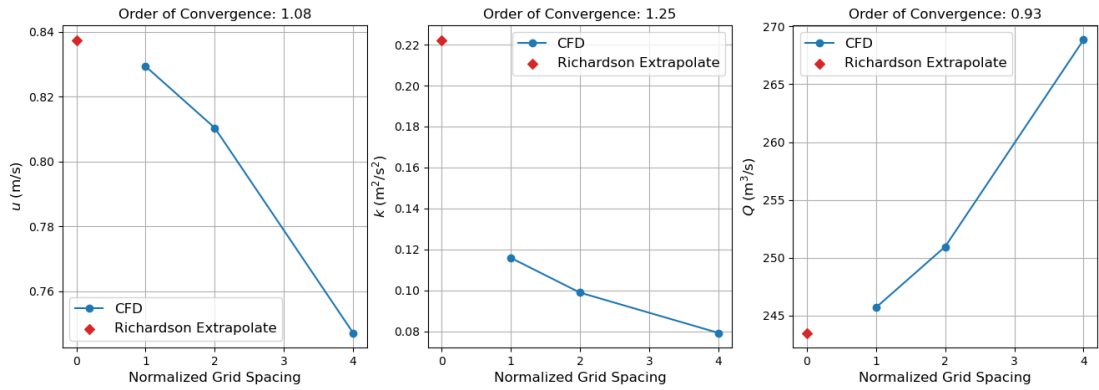


Figure 3.5: **[EN]** Results of Richardson extrapolation for (from left to right) velocity magnitude, turbulent kinetic energy and discharge. **[NL]** Het resultaat van Richardson extrapolatie voor (van links naar rechts) stroomsnelheid, turbulente kinetische energie en afvoer.

Another approach to determine the stability of numerical solutions is the Courant number C ,

$$C = \frac{|U|\Delta t}{\Delta x}, \quad (3.1)$$

with velocity magnitude $|U|$, timestep Δt and grid size Δx . The Courant–Friedrichs–Lewy (CFL) condition states that, generally, stable solutions must have a Courant number less than or equal to 1. STAR-CCM+'s implicit solver however does not require a Courant number $C < 1$ for numerical stability. In this case, $C < 1$ everywhere except in the jet(s) originating from the weir in the higher discharge cases, such as S330, where $C \leq 5$ (see Figure 3.6).

Simcenter STAR-CCM+

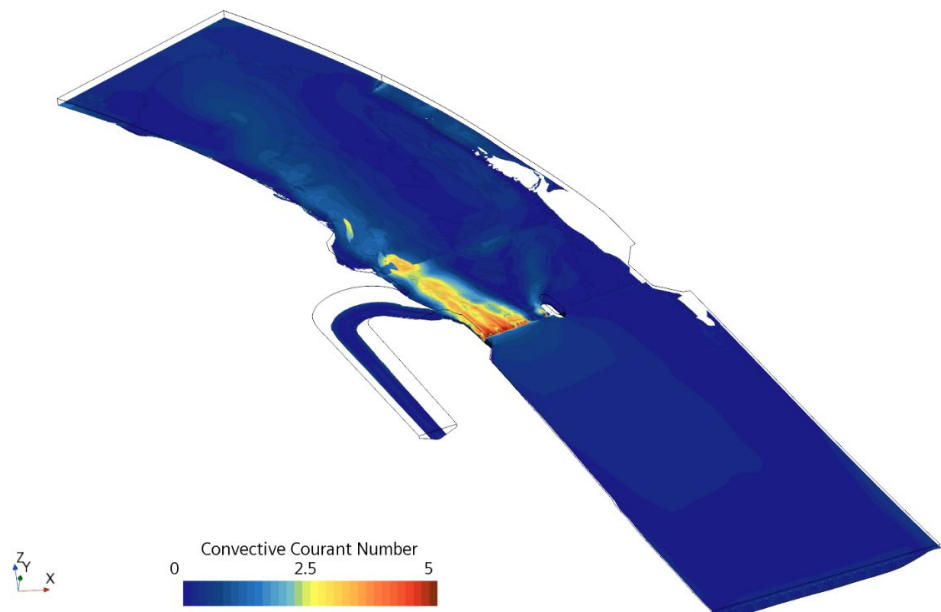


Figure 3.6: **[EN]** Overview of the Courant numbers within the numerical domain for simulation S330 (see Table 3.1). **[NL]** Overzicht van de Courant getallen in het domein van simulatie S330.

3.4 Validation based on field measurements

Rijkswaterstaat performed ADCP field measurements near weir Grave on June 19th, 2024. They measured velocities up- and downstream of weir Grave and at several locations in the

fishway. The measurement campaign was carried out during a Meuse discharge of approximately $Q \approx 330 \text{ m}^3/\text{s}$. Due to ongoing maintenance on the large weir, most of the discharge flowed through the small weir (i.e. the weir nearest to the fishway). The average of the velocity profiles that were measured in the fishway is used as a velocity boundary condition in the fishway (see Section 3.2). The velocity fields that were measured near the outflow of the fishway and in the main river section will be used for validation of the 3D CFD model described in Sections 3.1 through 3.3.

3.4.1 Conditions in the field

The larger of the two weirs was undergoing maintenance at the time of the field measurements, which meant that there were boats and pontoons just downstream of that weir. Regular weir operation was therefore not in effect. Strong turbulence was observed near the fishway due to these unusual circumstances (see Figure 3.7).



Figure 3.7: **[EN]** Whitewater near the fishway entrance ($Q \approx 330 \text{ m}^3/\text{s}$ through the small Poirée weir, June 19th, 2024). **[NL]** Turbulente stroming nabij de vistrapingang ($Q \approx 330 \text{ m}^3/\text{s}$ door de kleine stuw, 19 juni 2024).

The weir configuration in the CFD model, shown in Figure 3.9, is based on pictures taken during the field measurements (Figure 3.8). It was assumed that all gates in the larger weir were placed, and that only gates in the smaller weir had been removed. The operators of weir Grave confirmed that ten gates were removed at the time of the field measurements but could not verify which gates had been removed specifically (personal communication, operator weir Grave, September 2024). There was approximately $330 \text{ m}^3/\text{s}$ of river discharge and $3.5 \text{ m}^3/\text{s}$ of fishway discharge at the time of the measurements. The measured river discharge is accurately reproduced by the CFD model. The water levels up- and downstream of the weir during these measurements were approximately $+7.80 \text{ m NAP}$ and $+5.00 \text{ m NAP}^2$, respectively.

² The water levels were retrieved from national monitoring network Landelijk Meetnet Water (LMW) at locations 'Grave boven' and 'Grave beneden' ([Waterhoogte - Rijkswaterstaat Waterinfo](#)).



Figure 3.8: **[EN]** View of the smaller weir at the time of the field measurements on June 19th, 2024. **[NL]** Aanzicht van de kleine stuw tijdens de veldmetingen op 19 juni 2024.

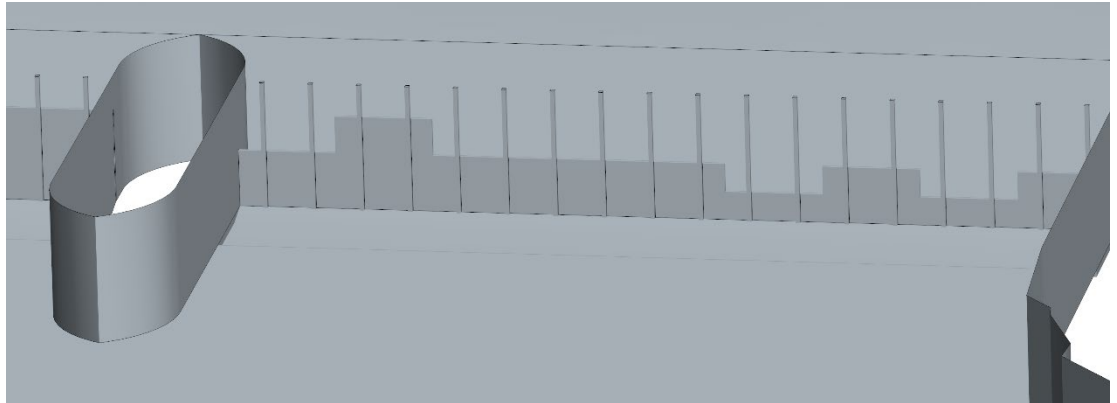


Figure 3.9: **[EN]** Weir configuration as implemented (based on Figure 3.8) in the validation calculations. **[NL]** Schuivenconfiguratie zoals toegepast in het validatiemodel (gebaseerd op Figure 3.8).

3.4.2 Velocity fields in the main river section

The riverbank on the left-hand side of the river was damaged during a calamity in 2016 where a ship collided with and damaged the weir. Initially, simulations were performed using a geometry that did not include the erosion recess in the riverbank. By comparing the resulting flow fields to the results of the study of the calamity (Deltares, 2018) and the measured velocity fields, it was found that this recess has a significant impact on the flow patterns. The geometry was therefore updated to include the recess and to simulate the flow patterns correctly. A comparison between simulations with and without the recess is shown in Figure 3.10. The recess causes the jet that originates from the smaller weir to separate from the left-hand riverbank and cross over towards the opposing riverbank. The newer model also shows that the ‘island’ in-between the main river and the navigation locks is not flooded – which is in accordance with the situation in the field.

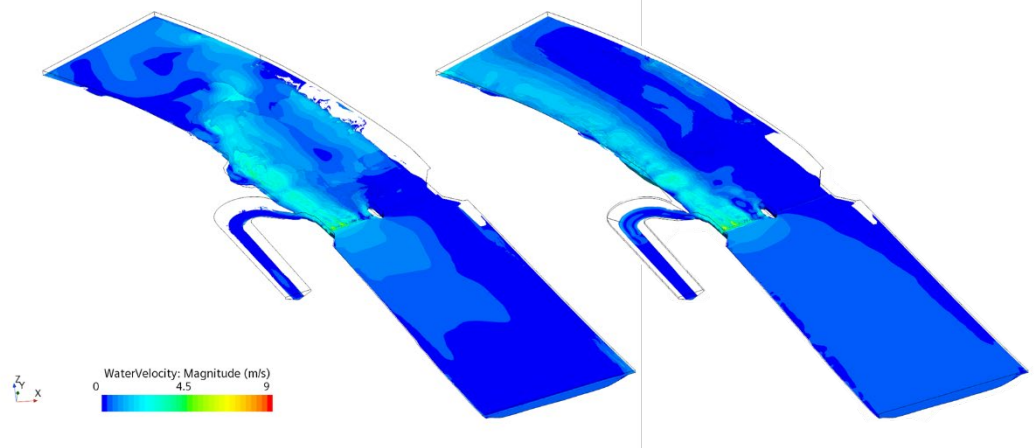
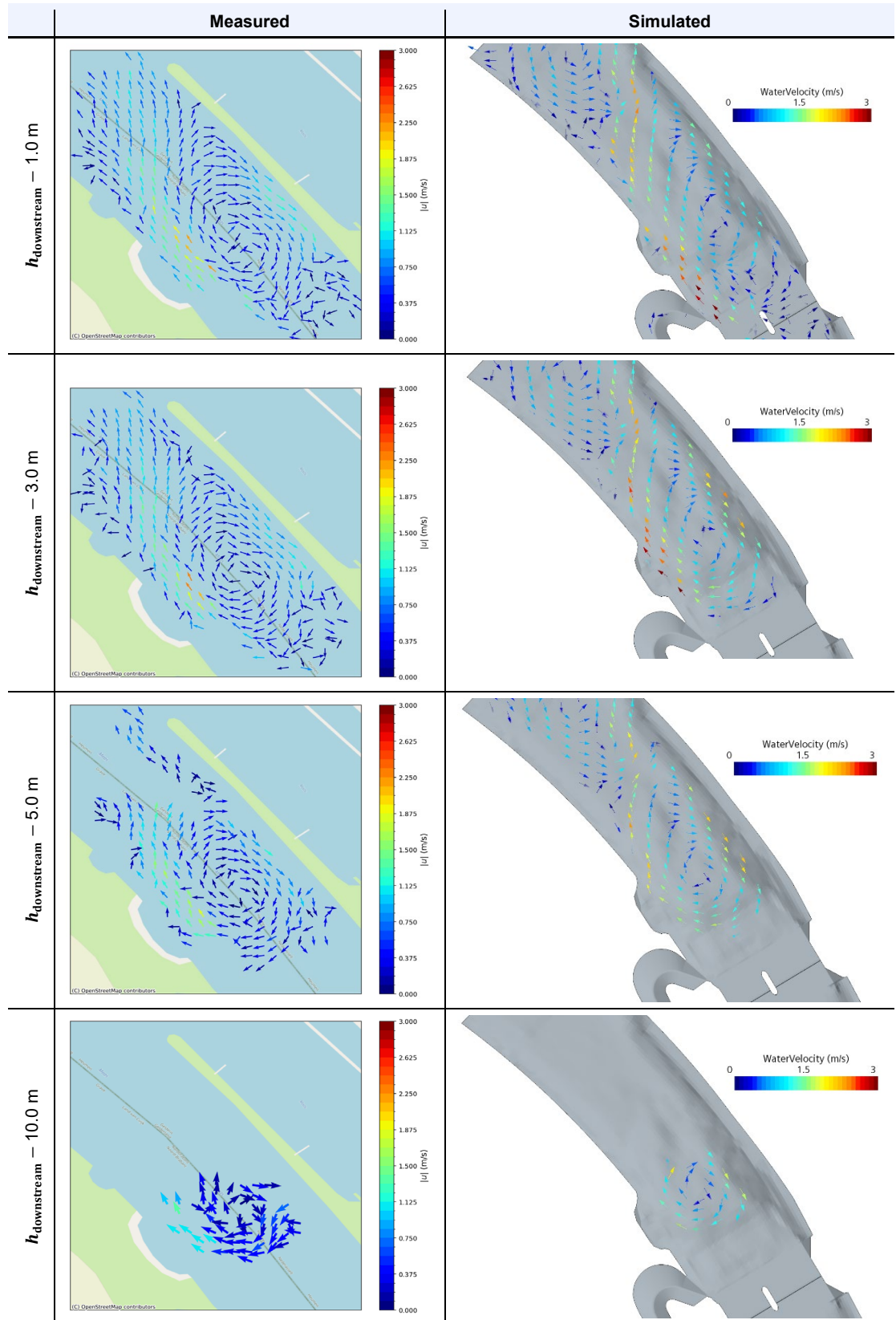


Figure 3.10: **[EN]** Velocity magnitude at the water surface in the geometry with (left) and without (right) the recess in the left-hand riverbank. **[NL]** Stroomsnelheden aan het wateroppervlak in de geometrie met (links) en zonder (rechts) erosiekuil aan de linkeroever.

Table 3.2 shows a comparison between the field measurements and CFD calculations of the velocity fields downstream of weir Grave:

- Qualitatively, CFD can accurately predict the flow structures.
 - Both the measured and calculated flow fields show how the jet that originates from the smaller weir crosses over to the other side of the river, and that a recirculation zone forms just to the right of this jet.
- Quantitatively, the simulated velocities overestimate the measured velocities.
 - At one metre below the water surface, the measured velocity in the jet is equal to at most 2.2 m/s (orange in Table 3.2), whereas the CFD calculations show velocities of up to 4.0 m/s (note that the figures are clipped at 3.0 m/s) in the jet. The overall maximum velocity in the field measurements occurs two metres below the water surface and is equal to 2.6 m/s.
 - The velocities in the core of the recirculation zone are similar, however the simulated velocities are greater than the measured velocities in the outer region of this zone. This is likely a consequence of the strong jet flow from the small weir that shears past the stagnant flow downstream of the large weir.

Table 3.2: Comparison between the field measurements and CFD calculations of the velocity downstream of weir Grave at different depths (with respect to the water surface) in the water column.



The size of the grid cells near the weir and free surface (0.25 m) and in the remaining numerical domain (0.50 m) are similar to the bin size that was used in the ADCP measurements (0.50 m). It is therefore expected that the chosen bin size does not contribute to this difference significantly. The water levels in the field measurements are defined with respect to the water surface. The velocity fields in CFD are also based on this reference, but the water level was not the same in the field as in the simulations. It must also be noted that the water levels in the field were retrieved² at a location farther downstream than the boundary on the numerical domain. The velocity profiles in Table 3.2 therefore do not show the exact same water level with respect to NAP, but with respect to the measured or simulated free surface level.

The difference between measured and calculated velocities is expected to (partly) be the result of the CFD model's inability to correctly resolve the shear between the strong jet flow through the small weir and the stagnant flow behind the large weir. The other simulated cases do not show this behaviour (see Table 3.1). To further validate the CFD model, it would be beneficial to perform validation measurements under regular weir operation. Strong turbulence (see Figure 3.7) may have negatively impacted the accuracy of the ADCP measurements (STOWA, 2009). The inaccuracies are likely only significant in shallow areas, if insufficient transects were made or if high boat velocities were used (Tarrab et al., 2012), which is not expected to be the case.

3.4.3 Velocity field in the fishway outflow

The velocity field in the outflow of the fishway was determined by averaging sixteen measured profiles. This averaged result is shown in Figure 3.11. The highest velocities are concentrated near one side of the fishway. This is the side that is closest to the bend in the fishway, where highest velocities are expected due to centrifugal forces. The velocity profile near the outflow in the CFD calculations (see Figure 3.12) also show the highest velocities in that same outer section, but there is a small region of very slow flow (dark blue in Figure 3.12) between the middle and outer section. On average, the calculated velocities in the middle section appear to be greater (≈ 0.7 m/s) than what was measured (≈ 0.4 m/s).

The exact geometry of the fishway is very uncertain (see Section 3.1) and several assumptions have been made in the CAD model. Based on the measured velocity profiles it appears that the bed of the fishway lies deeper (+2.75 m NAP) in the simulations than what was measured, although it must also be noted that ADCP measurements have a 'blank' area near the water surface and near the riverbed due to sensor placement and interference, respectively. The exact water depth therefore cannot be determined from the measurements. Because of this, it is not entirely unexpected or surprising that these profiles do not match well.

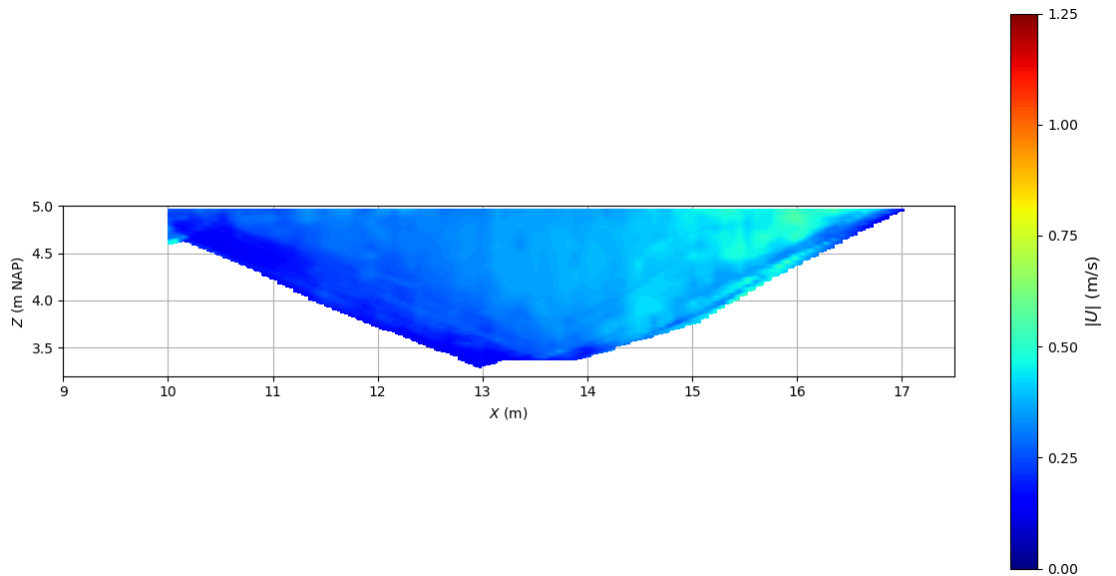


Figure 3.11: **[EN]** Velocity magnitude at a cross-section of the fishway near the outflow, averaged over sixteen measured velocity profiles. **[EN]** Stroomsnelheden in een doorsnede van de vistrap nabij de uitstroom, gemiddeld over zestien gemeten profielen.

Simcenter STAR-CCM+

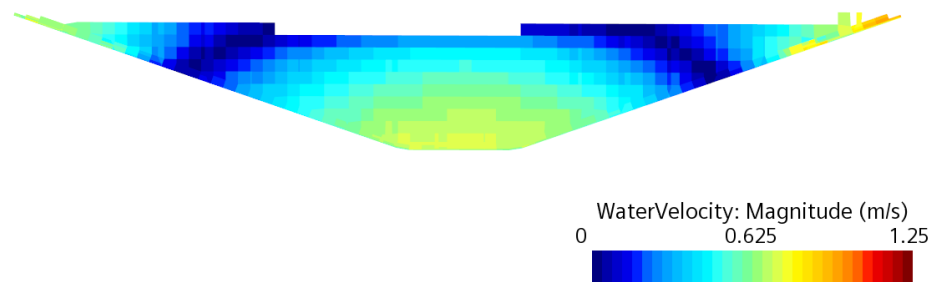


Figure 3.12: **[EN]** Velocity magnitude at a cross-section of the fishway near the outflow, as calculated in the CFD model. **[NL]** Stroomsnelheden in een doorsnede van de vistrap nabij de uitstroom, zoals berekend in het CFD model.

4 Results

This chapter describes the results of the CFD simulations. The interpretations are based on juvenile European eel (from now on referred to as glass eel) and adult Atlantic salmon (from now on referred to as salmon). Section 4.1 discusses the magnitude of attraction flow and the relevance of the different discharge scenarios for both fish species. The velocity magnitude is then analysed per fish species (Section 4.2), and lastly the turbulent parameters are analysed for fish in general (Section 4.3). Please note that all figures of flow patterns are snapshots from flow that varies in time. The flow patterns do not change significantly from one second to the next, and as such these snapshots are considered sufficient for the analysis below.

4.1 Discharge ratio

The discharge ratio criterion (approximately 1 – 5% (Larinier, 2002), see Section 2.1.1) suggests that the available maximum fishway discharge of 4 m³/s is insufficient whenever the river discharge is greater than 400 m³/s. Figure 4.1 shows the average Meuse discharge for different climate scenarios, and how the occurrence of the different average discharges overlap with the migration seasons of glass eel and salmon.

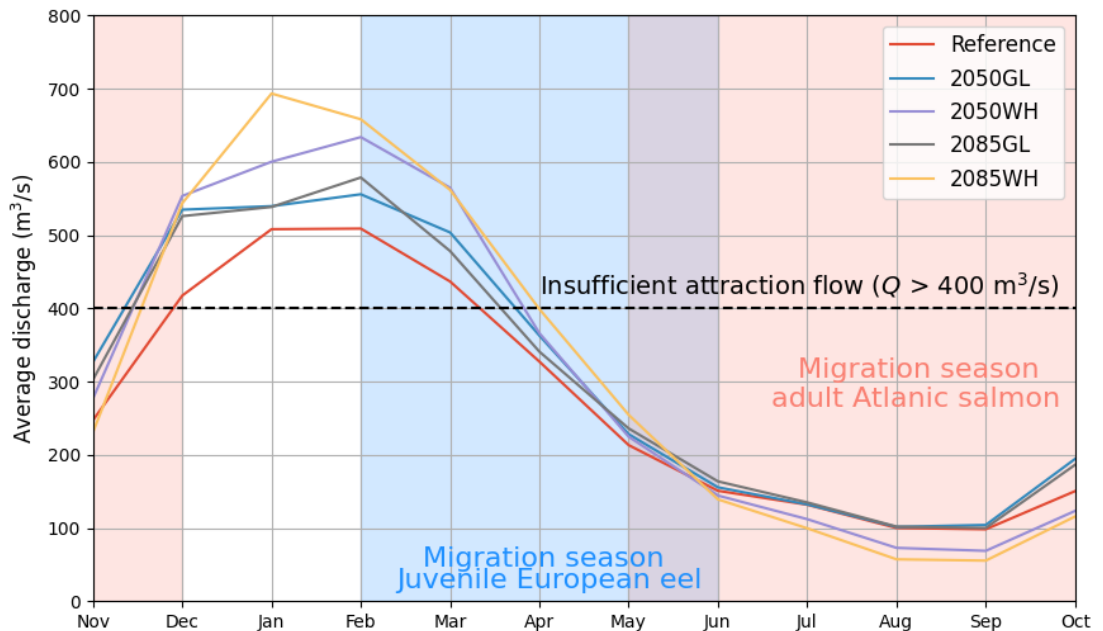


Figure 4.1: [EN] Average Meuse discharge per month for different climate scenarios (KpNK, 2022). The highlighted areas indicate the migration season for glass eel (blue) and salmon (pink). [NL] Gemiddelde Maasafvoer per maand in verschillende klimaatscenario's. De gearceerde vlakken markeren het typische migratie seizoen van glasaal (blauw) en zalm (roze).

From Figure 4.1, it becomes clear that the attraction flow may be insufficient during February to mid-March for glass eel. For salmon, only the period mid-November to December may have insufficient attraction flow. In practice, during the field measurements, only 3.5 m³/s was measured in the fishway. This would shift the insufficient attraction flow down to scenarios with 350 m³/s or more. This affects both species: for glass eel the period with insufficient attraction flow expands to mid-March to April, for salmon it expands to early to mid-November.

It must be kept in mind that this criterion alone cannot judge whether the magnitude of the attraction flow is satisfactory: Larinier (2002) also acknowledges that an incorrect fishway entrance position means that attraction flows must be higher than the minimum of 1 – 5% of the river discharge (see Section 2.1.2).

4.2 Velocity

The velocity magnitude just downstream of weir Grave is presented using the colour scale as used by Gisen et al. (2017): the colours purple, green, yellow and red represent the non-rheoactive, sustained, prolonged and burst velocities, respectively (see Figure 4.2). The migration limit line can be visualised as the outline of the red region (burst). The continuous migration corridor is the combination of the green and yellow regions (sustained and prolonged). In the following sections, all simulated scenarios will be interpreted using the swimming performance of glass eel and salmon, and conclusions will be drawn on whether or not a continuous migration corridor exists during their migration period (see Figure 4.1).

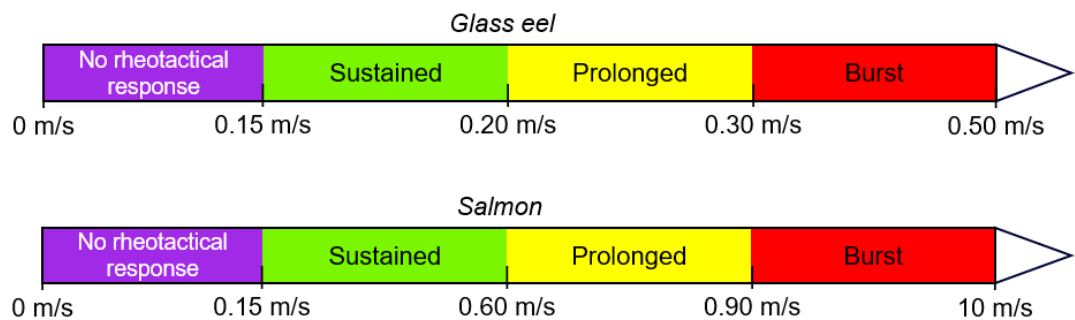


Figure 4.2: **[EN]** Colour classification for non-rheoactive, sustained, prolonged and burst velocities of glass eel and salmon. **[NL]** Kleurenindeling voor niet-aantrekkende, langdurig vol te houden, en sprintsnelheden van glasaal en zalm.

4.2.1 European eel

Figure 4.3 through Figure 4.7 show the velocities downstream of weir Grave for scenarios S100, S100L, S100R, S250 and S330, respectively, interpreted for the swimming performance of glass eel (see Table 2.1). Any transparent areas in the shown cross-sections indicate that the velocities are even greater than the (red) burst velocities.

Simcenter STAR-CCM+

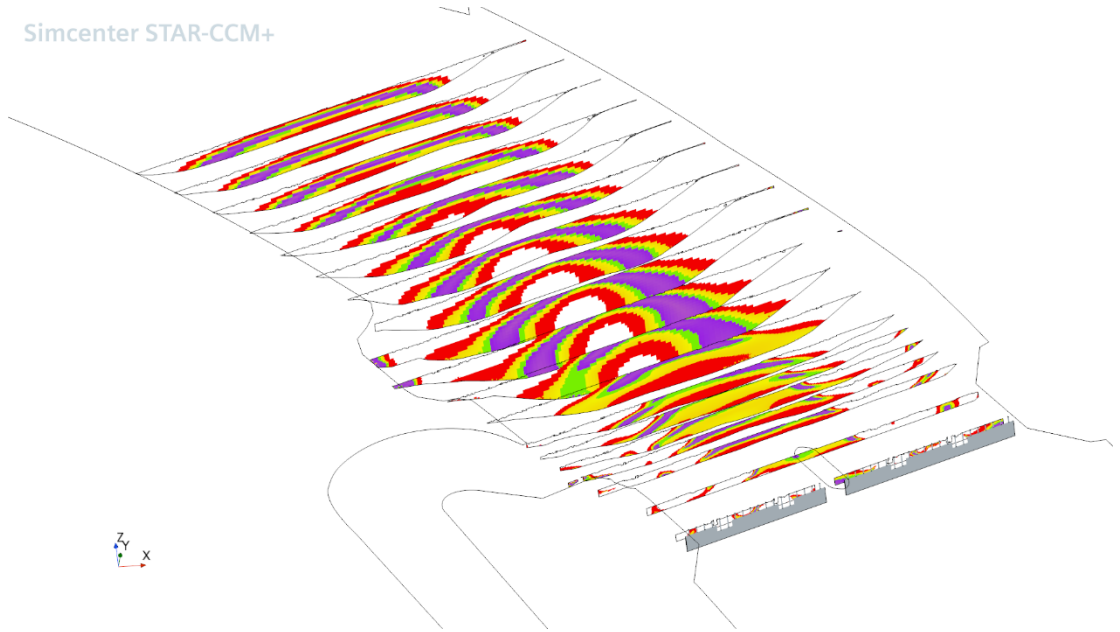


Figure 4.3: **[EN]** Flow velocities downstream of weir Grave in scenario S100, where green and yellow are the continuous migration corridor, and the outline of the red region is the migration limit line for glass eel. **[NL]** Stroomsnelheden benedenstrooms van stuw Grave in scenario S100, waar groen en geel het continue migratiepad markeert, en de grenzen van het rode gebied de migratielimitlijn voorstelt voor glasaal.

Simcenter STAR-CCM+

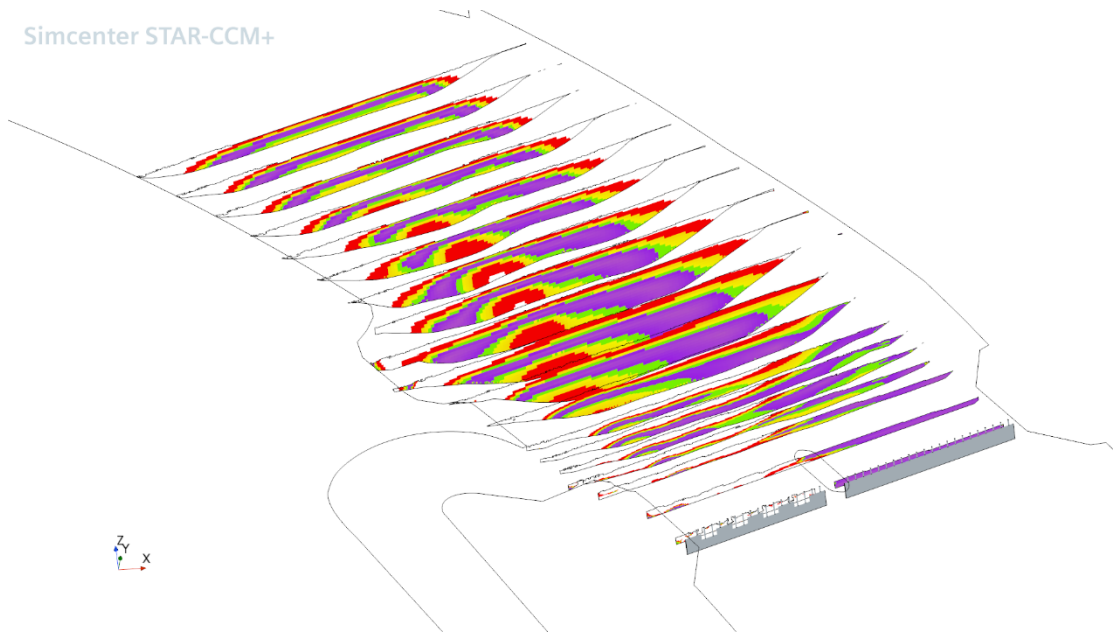


Figure 4.4: **[EN]** Flow velocities downstream of weir Grave in scenario S100L, where green and yellow are the continuous migration corridor, and the outline of the red region is the migration limit line for glass eel. **[NL]** Stroomsnelheden benedenstrooms van stuw Grave in scenario S100L, waar groen en geel het continue migratiepad markeert, en de grenzen van het rode gebied de migratielimitlijn voorstelt voor glasaal.

Simcenter STAR-CCM+

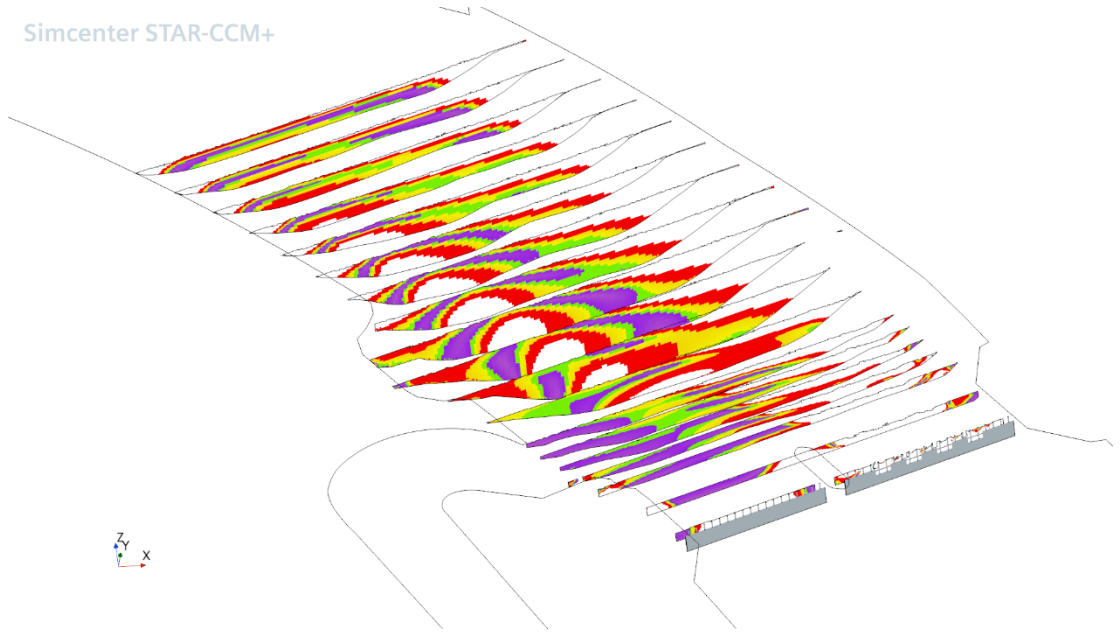


Figure 4.5: **[EN]** Flow velocities downstream of weir Grave in scenario S100R, where green and yellow are the continuous migration corridor, and the outline of the red region is the migration limit line for glass eel. **[NL]** Stroomsnelheden benedenstrooms van stuw Grave in scenario S100R, waar groen en geel het continue migratiepad markeert, en de grenzen van het rode gebied de migratielimitlijn voorstelt voor glasaal.

Simcenter STAR-CCM+

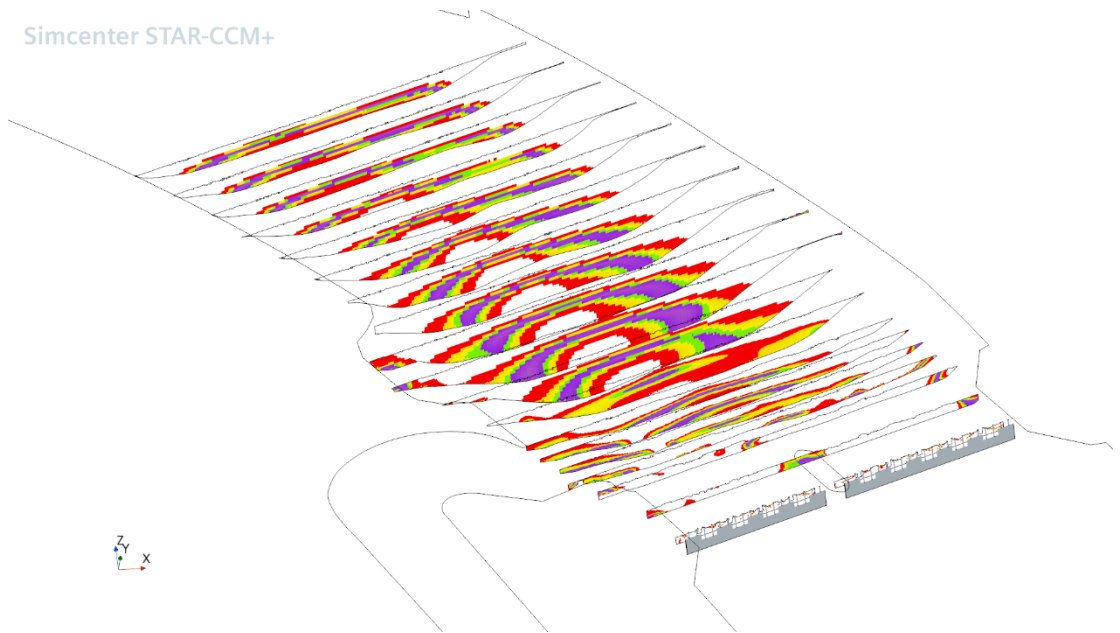


Figure 4.6: **[EN]** Flow velocities downstream of weir Grave in scenario S250, where green and yellow are the continuous migration corridor, and the outline of the red region is the migration limit line for glass eel. **[NL]** Stroomsnelheden benedenstrooms van stuw Grave in scenario S250, waar groen en geel het continue migratiepad markeert, en de grenzen van het rode gebied de migratielimitlijn voorstelt voor glasaal.

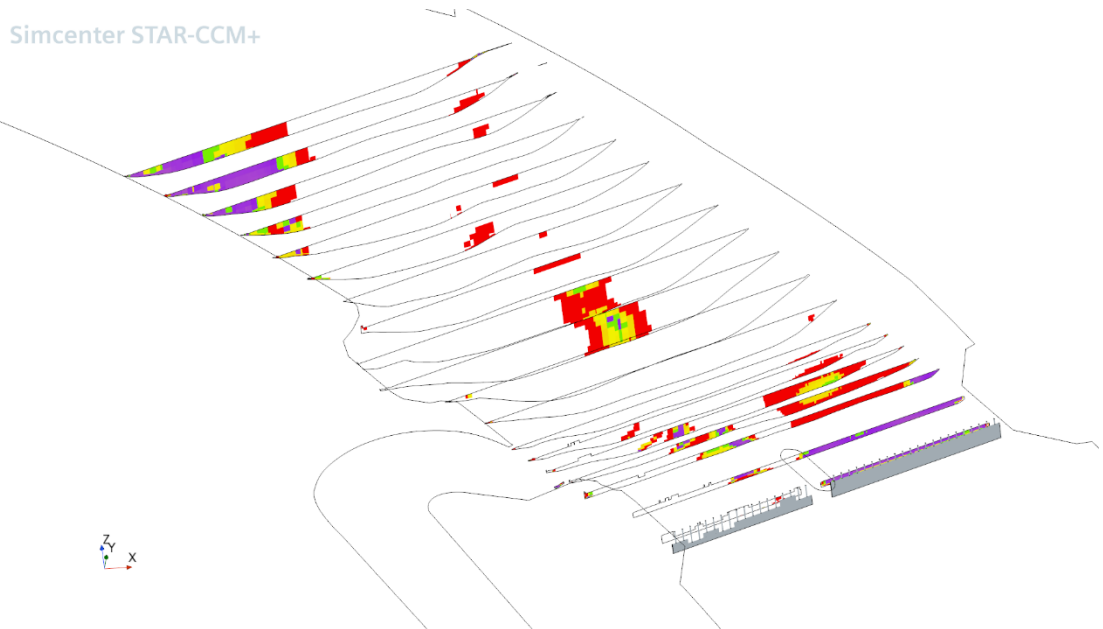


Figure 4.7: **[EN]** Flow velocities downstream of weir Grave in scenario S330, where green and yellow are the continuous migration corridor, and the outline of the red region is the migration limit line for glass eel. **[NL]** Stroomsnelheden benedenstrooms van stuw Grave in scenario S330, waar groen en geel het continue migratiepad markeert, en de grenzen van het rode gebied de migratielimietslijn voorstelt voor glasaal.

Figure 4.3 through Figure 4.7 show that there are no continuous migration corridors based on the swimming performance of glass eel in almost all scenarios. There are many regions that even exceed the burst velocity of glass eel (shown as transparent), including the region of interest right in front of the fishway. The only exception is S100R, where a complicated (narrow and winding) green-yellow route can be seen. Part of this route is located close to the water surface and seeing as glass eel are bottom-dwelling fish (Veza et al., 2020), it is expected that this route does not contribute to “good” findability. Especially so because of the large area of non-rheoactive (and therefore non-attractive) velocities near the fishway entrance.

Figure 4.1 showed that glass eel typically migrates at discharges greater than $100 \text{ m}^3/\text{s}$. The fact that the CFD simulations have shown that glass eel already cannot overcome the velocities at $100 \text{ m}^3/\text{s}$ indicates that the fishway findability is too low for this species in all relevant discharge scenarios.

4.2.2 Atlantic salmon

Figure 4.8 through Figure 4.12 show the velocities downstream of weir Grave for scenarios S100, S100L, S100R, S250 and S330, respectively, interpreted for the swimming performance of salmon (see Table 2.1).

Simcenter STAR-CCM+

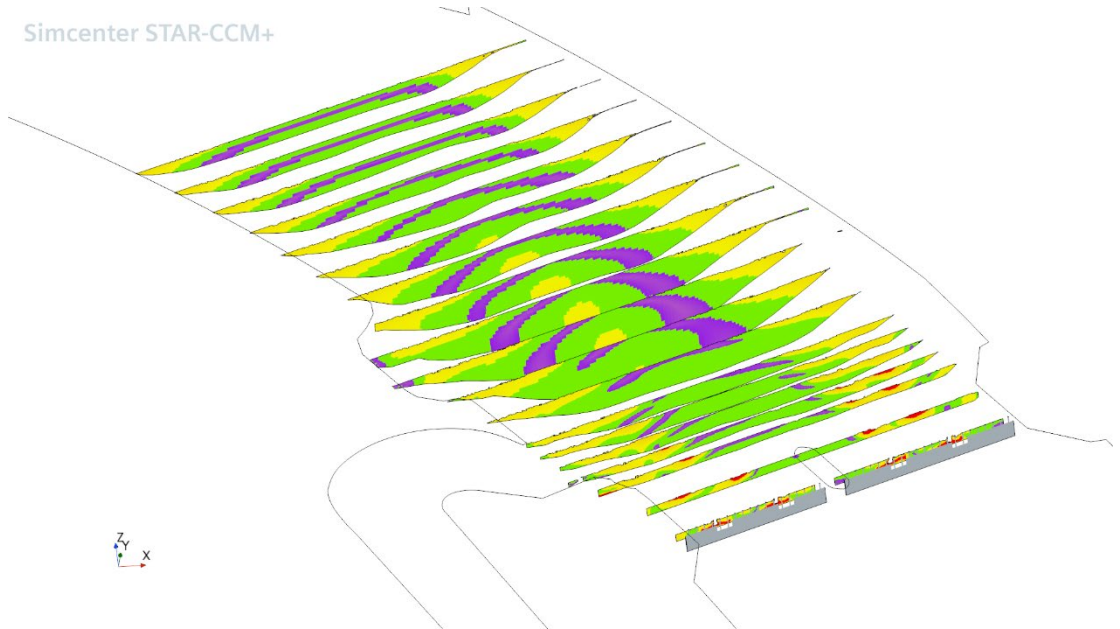


Figure 4.8: **[EN]** Flow velocities downstream of weir Grave in scenario S100, where green and yellow are the continuous migration corridor, and the outline of the red region is the migration limit line for salmon. **[NL]** Stroomsnelheden benedenstrooms van stuw Grave in scenario S100, waar groen en geel het continue migratiepad markeert, en de grenzen van het rode gebied de migratielimitlijn voorstelt voor zalm.

Simcenter STAR-CCM+

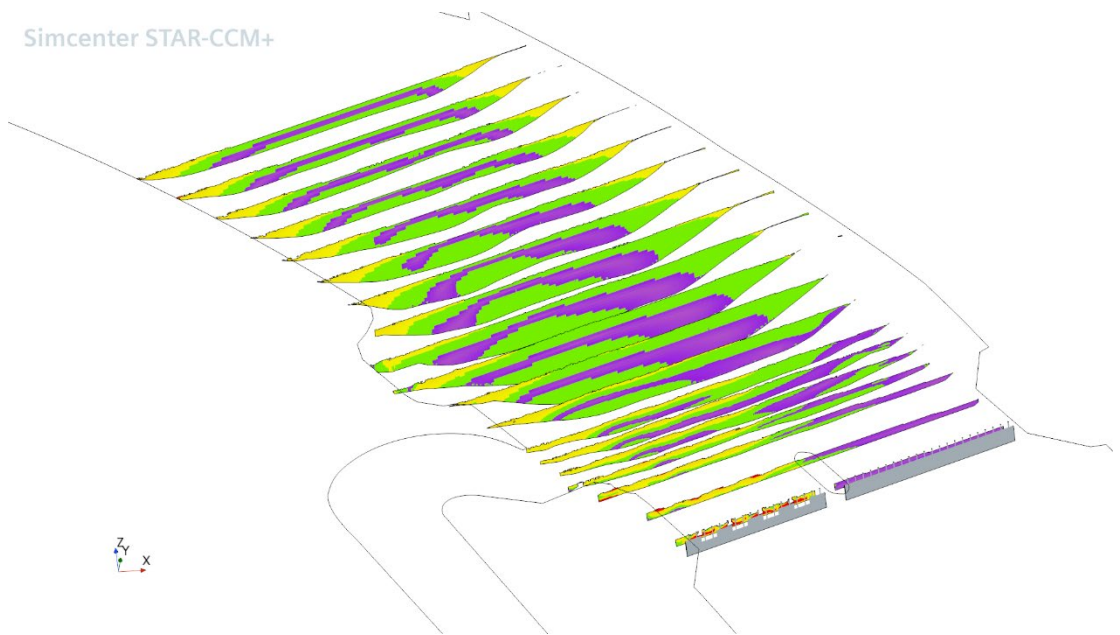


Figure 4.9: **[EN]** Flow velocities downstream of weir Grave in scenario S100L, where green and yellow are the continuous migration corridor, and the outline of the red region is the migration limit line for salmon. **[NL]** Stroomsnelheden benedenstrooms van stuw Grave in scenario S100L, waar groen en geel het continue migratiepad markeert, en de grenzen van het rode gebied de migratielimitlijn voorstelt voor zalm.

Simcenter STAR-CCM+

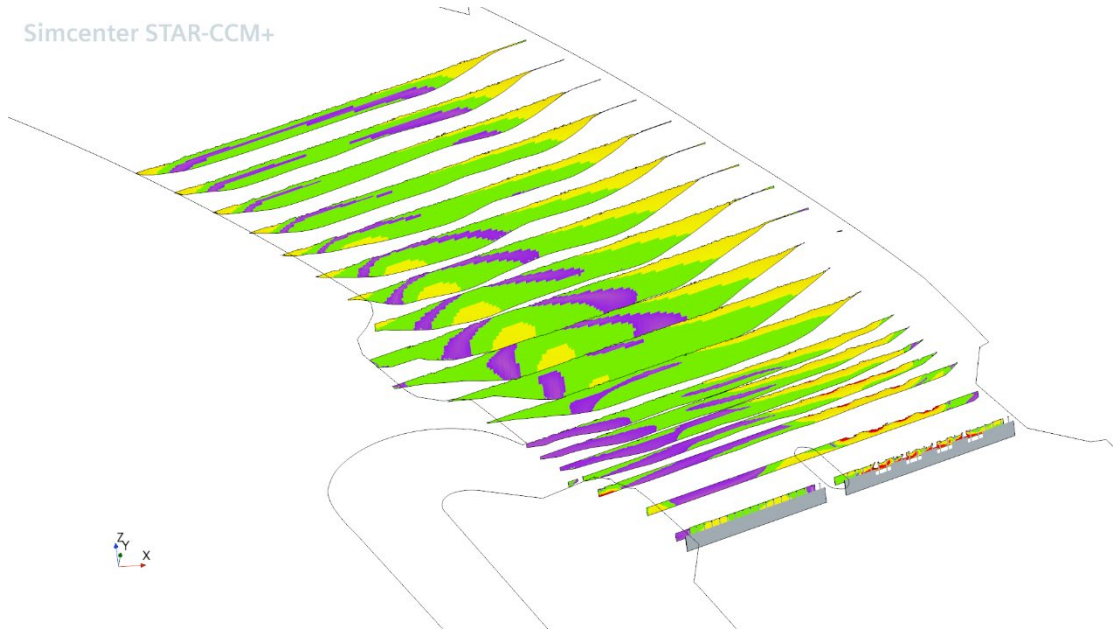


Figure 4.10: **[EN]** Flow velocities downstream of weir Grave in scenario S100R, where green and yellow are the continuous migration corridor, and the outline of the red region is the migration limit line for salmon. **[NL]** Stroomsnelheden benedenstrooms van stuw Grave in scenario S100R, waar groen en geel het continue migratiepad markeert, en de grenzen van het rode gebied de migratielimitlijn voorstelt voor zalm.

Simcenter STAR-CCM+

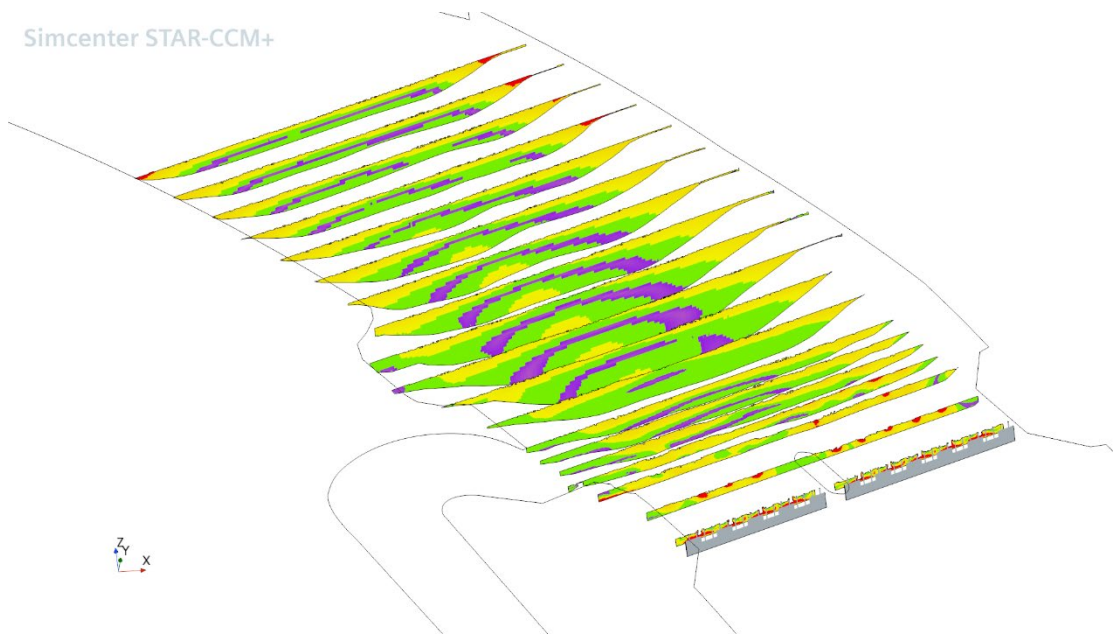


Figure 4.11: **[EN]** Flow velocities downstream of weir Grave in scenario S250, where green and yellow are the continuous migration corridor, and the outline of the red region is the migration limit line for salmon. **[NL]** Stroomsnelheden benedenstrooms van stuw Grave in scenario S250, waar groen en geel het continue migratiepad markeert, en de grenzen van het rode gebied de migratielimitlijn voorstelt voor zalm.

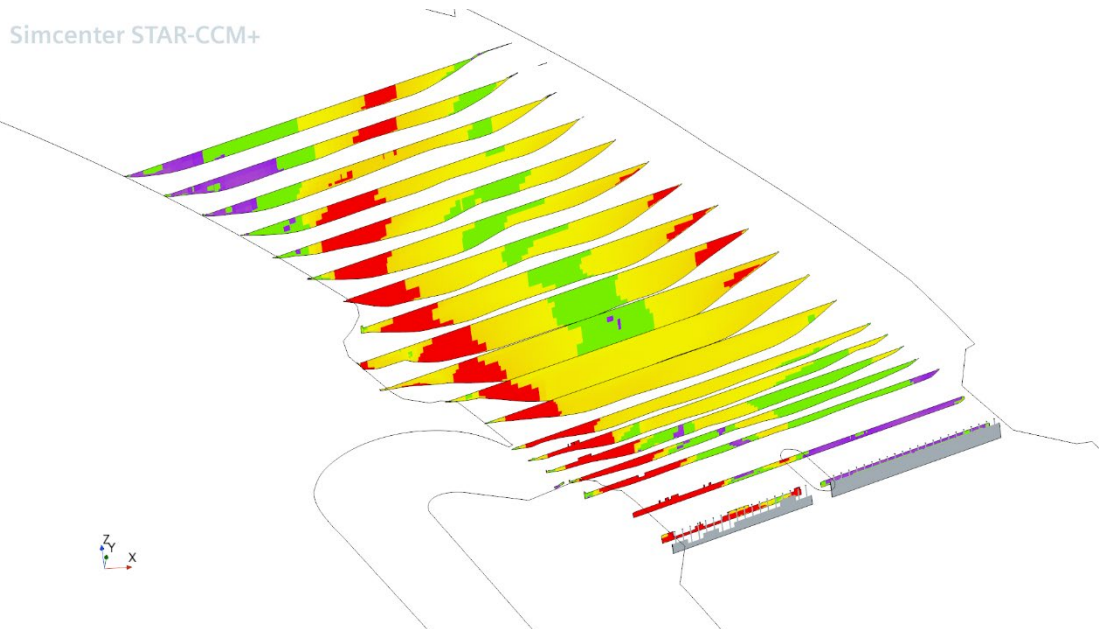


Figure 4.12: **[EN]** Flow velocities downstream of weir Grave in scenario S330, where green and yellow are the continuous migration corridor, and the outline of the red region is the migration limit line for salmon. **[NL]** Stroomsnelheden benedenstrooms van stuw Grave in scenario S330, waar groen en geel het continue migratiepad markeert, en de grenzen van het rode gebied de migratielimitlijn voorstelt voor zalm.

Figure 4.8 through Figure 4.12 show that there are continuous migration corridors based on the swimming performance of salmon in all scenarios except S330. Scenario S100R is less straightforward: it introduces some velocities that are too low for salmon to be attracted in that direction (purple). There is a green region close to the water surface that crosses over from the middle of the river towards the fishway, but there is also a yellow region (meaning greater velocity) to the left of the river that salmon may be more likely to follow, as fish will follow the strongest possible flow as long as possible (see Chapter 2). This area of strongest flow coincides with a turbulent area, which may lead the salmon away from this area and towards the fishway. Swimming against strong flow will fatigue the fish and combined with a very weak attraction flow to attract the fish in the right direction, this will likely result in the fish not being able to pass at all. A definitive estimation of the fishway findability in S100R is therefore not so straightforward. In cases such as these, it seems that having fishways on both sides of the river would be beneficial, but the turbulence in that region would likely have prevented the salmon from reaching the entrance on that side (see Section 4.3.1 and Figure 4.16).

In scenario S330, there is no continuous migration corridor visible for salmon (see Figure 4.12). The velocities in the strong jet originating from the weir (also see Section 3.4.2 and Figure 3.10) are in the 'burst' range for salmon. These velocities could only be passed if the region can be crossed in less than twenty seconds (see Section 2.2.1). The jet is approximately twenty metres wide and the trajectory the fish swims might be longer and not directly from left to right. Another advantage that this species has, is the ability to jump to overcome obstacles (Baudoin, et al., 2014). Combining these two types of locomotion might help this species to pass higher discharges, but this is outside of the scope of this analysis. It is therefore not ruled out that the jet could possibly be passed by salmon.

The entire 330 m³/s is concentrated through a single weir, so these results do not necessarily mean that salmon cannot reach the fishway during this river discharge. An equally distributed weir configuration could alter the flow pattern to benefit the salmon. Salmon also migrate at discharges greater than the highest simulated discharge (up to ≈550 m³/s, see Figure 4.1), but due to the concentrated beam in S330, it should not necessarily be concluded that there are

no weir configurations possible to create satisfactory flow patterns for salmon at discharges greater than 330 m³/s.

From the validation case (see Section 3.4.2) we also know that the velocities in the jet were overestimated by CFD. The measured velocity fields (see Table 3.2) show that salmon's burst velocities only occur in a four metres thick layer below the surface (in the jet), and that the velocities away from the surface are within salmon's sustained and prolonged swimming capacity. This suggests that there might have been a continuous migration corridor available in terms of flow velocities, but the field measurements unfortunately did not capture the velocities right in front of the fishway entrance (see Figure 4.13). What stands out by comparing Figure 4.12 and Figure 4.13 is that the area of 'prolonged' (yellow) velocities in the CFD model was mostly 'sustained' (green) in the field. Both of these velocities are navigable for salmon, and as such the overall conclusion for this scenario does not change based on the available information.

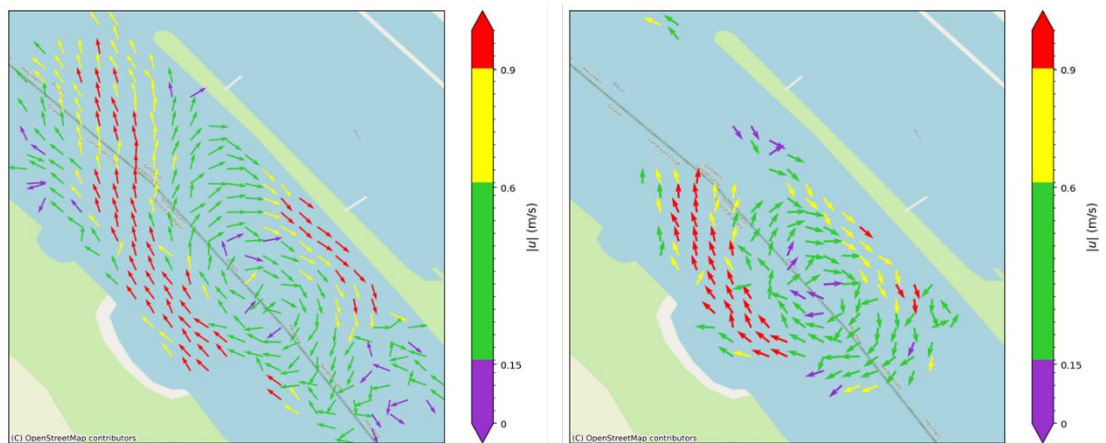


Figure 4.13: **[EN]** The swimming capacity colour classification applied to the field measurements at 1 metre (left) and 6 metres (right) below the water surface. **[NL]** De zwemprestatie kleurindeling toegepast op de veldmetingen op één meter (links) en zes meter (rechts) onder het water oppervlak.

Note that the existence of continuous migration corridors up to at least 250 m³/s (symmetrically divided over the weir) does not mean that salmon will thrive in the Meuse: there must also be suitable habitat and available food sources. Salmon and many other fish species are rheophilic (flow-loving) fish, and weirs cause a lack of flow by keeping in most of the water.

4.3 Turbulence

4.3.1 Turbulent kinetic energy

The migration limit line can be visualised as the outline of the red region (too turbulent), and the continuous migration corridor is the green region (passable turbulence). Figure 4.14 through Figure 4.18 show the turbulent kinetic energy downstream of weir Grave for scenarios S100, S100L, S100R, S250 and S330, respectively.

Simcenter STAR-CCM+

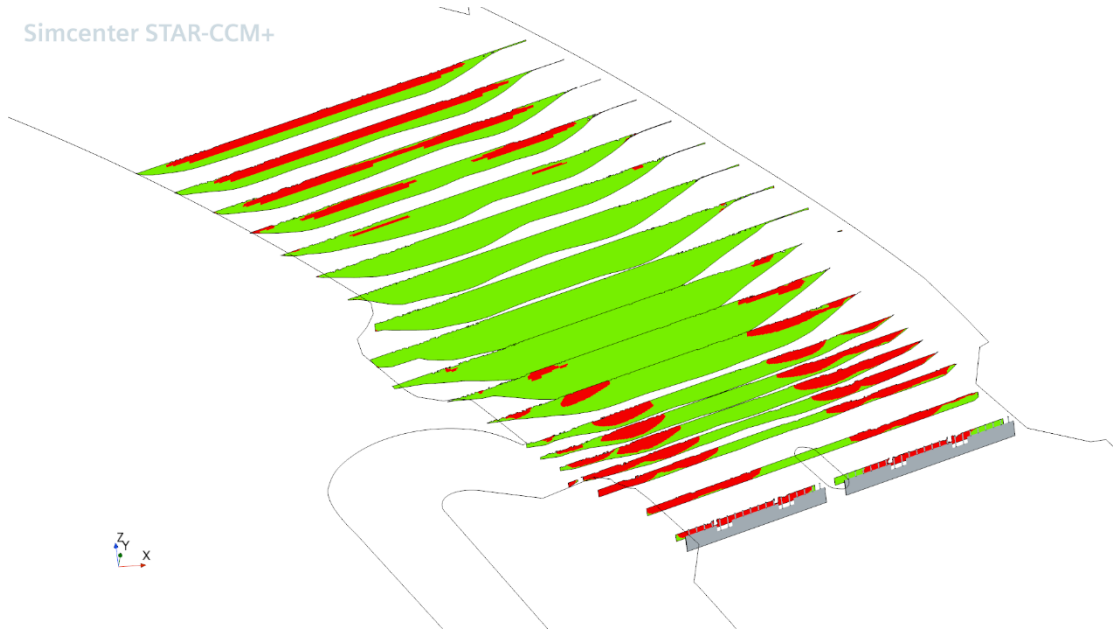


Figure 4.14: **[EN]** Turbulent kinetic energy downstream of weir Grave in scenario S100, where green indicates $k < 0.05 \text{ m}^2/\text{s}^2$ (passable turbulence) and red indicates $k \geq 0.05 \text{ m}^2/\text{s}^2$ (too strong turbulence). **[NL]** Turbulente kinetische energie benedenstrooms van stuw Grave in scenario S100, met $k < 0.05 \text{ m}^2/\text{s}^2$ (voldoende lage turbulentie) in het groen en $k \geq 0.05 \text{ m}^2/\text{s}^2$ (te sterke turbulentie) in het rood.

Simcenter STAR-CCM+

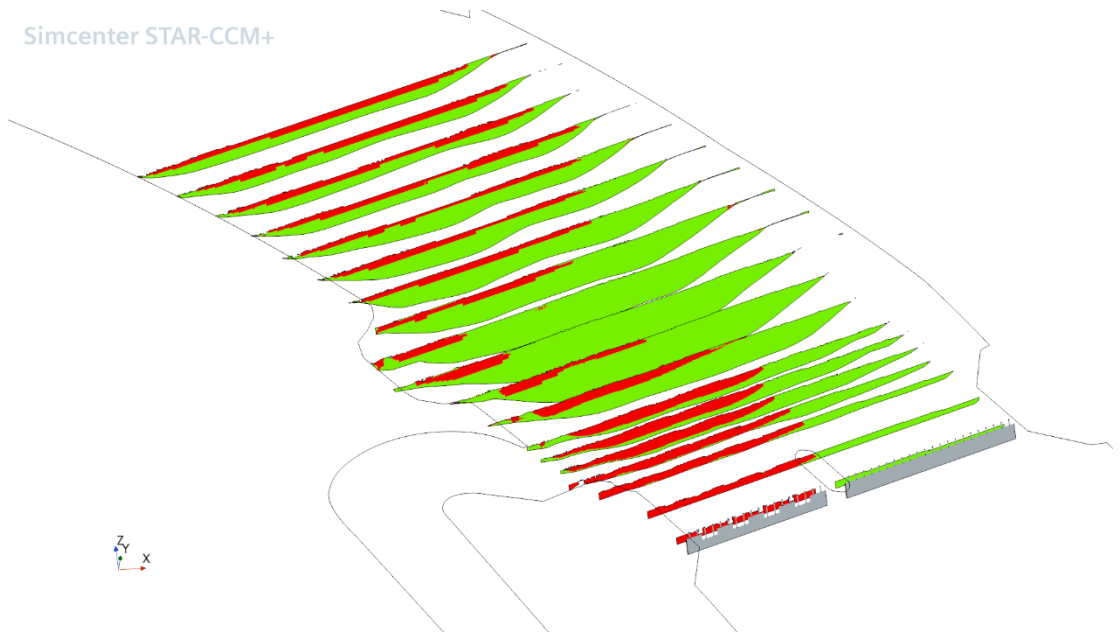


Figure 4.15: **[EN]** Turbulent kinetic energy downstream of weir Grave in scenario S100L, where green indicates $k < 0.05 \text{ m}^2/\text{s}^2$ (passable turbulence) and red indicates $k \geq 0.05 \text{ m}^2/\text{s}^2$ (too strong turbulence). **[NL]** Turbulente kinetische energie benedenstrooms van stuw Grave in scenario S100L, met $k < 0.05 \text{ m}^2/\text{s}^2$ (voldoende lage turbulentie) in het groen en $k \geq 0.05 \text{ m}^2/\text{s}^2$ (te sterke turbulentie) in het rood.

Simcenter STAR-CCM+

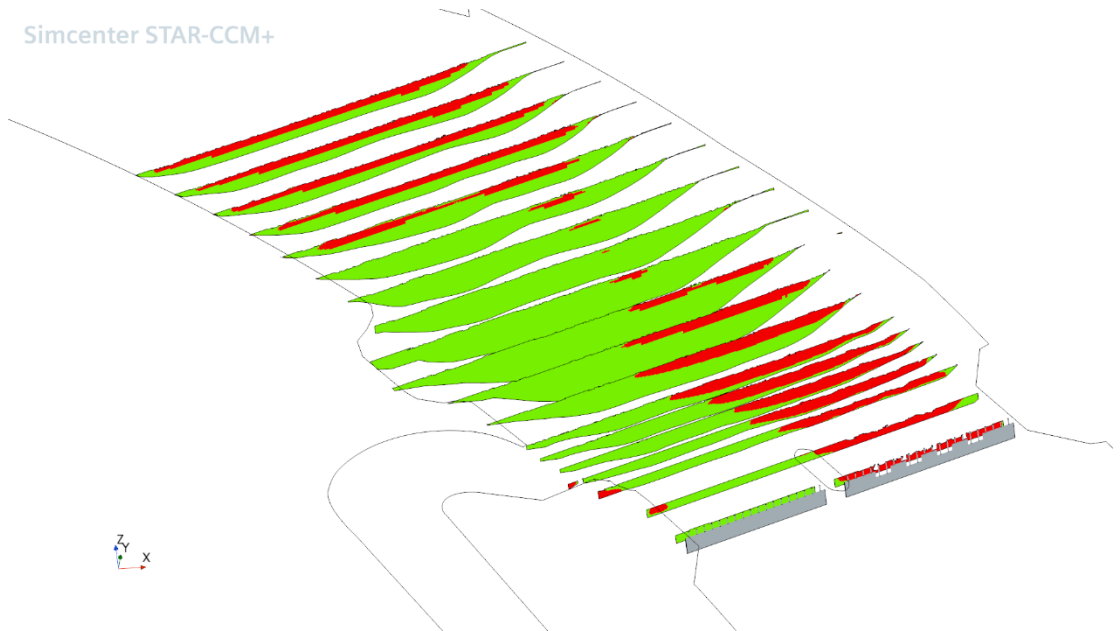


Figure 4.16: **[EN]** Turbulent kinetic energy downstream of weir Grave in scenario S100R, where green indicates $k < 0.05 \text{ m}^2/\text{s}^2$ (passable turbulence) and red indicates $k \geq 0.05 \text{ m}^2/\text{s}^2$ (too strong turbulence). **[NL]** Turbulente kinetische energie benedenstrooms van stuw Grave in scenario S100R, met $k < 0.05 \text{ m}^2/\text{s}^2$ (voldoende lage turbulentie) in het groen en $k \geq 0.05 \text{ m}^2/\text{s}^2$ (te sterke turbulentie) in het rood.

Simcenter STAR-CCM+

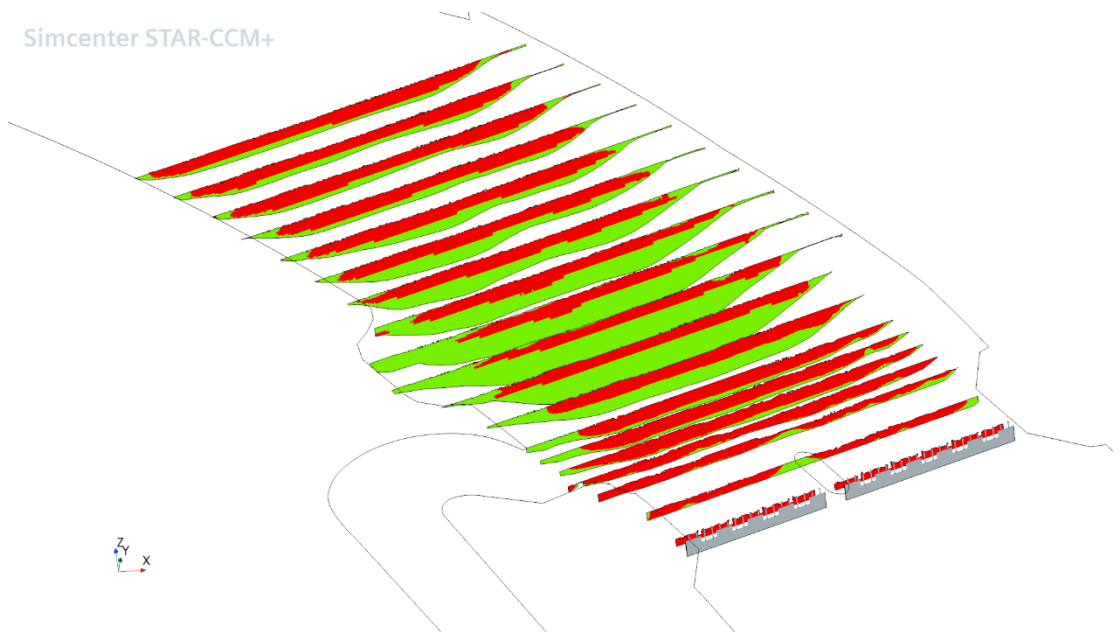


Figure 4.17: **[EN]** Turbulent kinetic energy downstream of weir Grave in scenario S250, where green indicates $k < 0.05 \text{ m}^2/\text{s}^2$ (passable turbulence) and red indicates $k \geq 0.05 \text{ m}^2/\text{s}^2$ (too strong turbulence). **[NL]** Turbulente kinetische energie benedenstrooms van stuw Grave in scenario S250, met $k < 0.05 \text{ m}^2/\text{s}^2$ (voldoende lage turbulentie) in het groen en $k \geq 0.05 \text{ m}^2/\text{s}^2$ (te sterke turbulentie) in het rood.

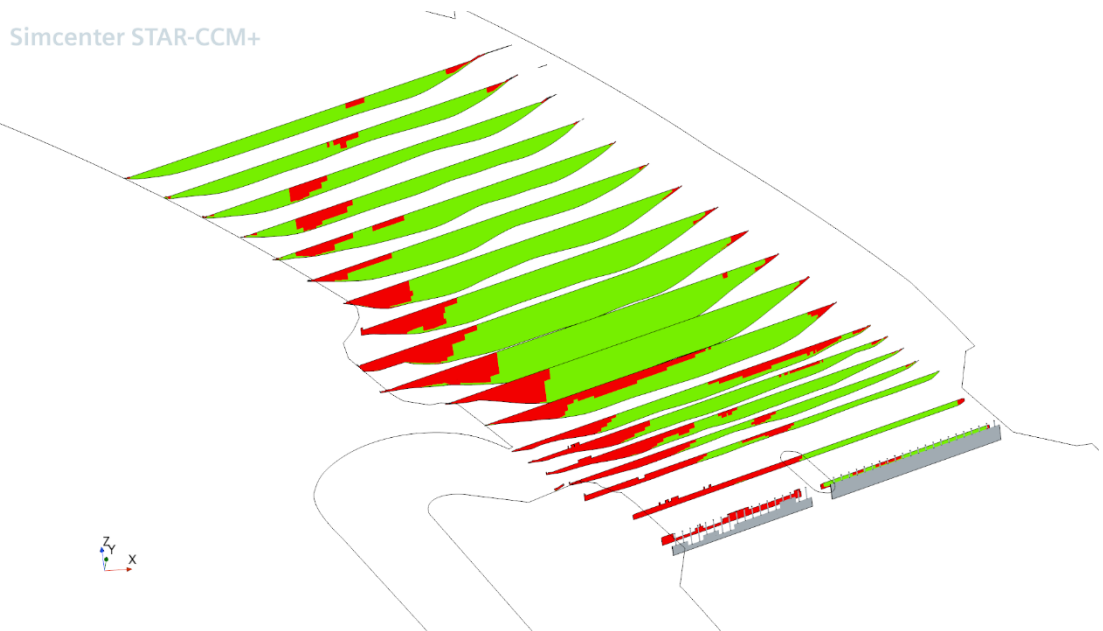


Figure 4.18: **[EN]** Turbulent kinetic energy downstream of weir Grave in scenario S330, where green indicates $k < 0.05 \text{ m}^2/\text{s}^2$ (passable turbulence) and red indicates $k \geq 0.05 \text{ m}^2/\text{s}^2$ (too strong turbulence). **[NL]** Turbulente kinetische energie benedenstrooms van stuw Grave in scenario S330, met $k < 0.05 \text{ m}^2/\text{s}^2$ (voldoende lage turbulentie) in het groen en $k \geq 0.05 \text{ m}^2/\text{s}^2$ (te sterke turbulentie) in het rood.

The turbulent kinetic energy limit ($k = 0.05 \text{ m}^2/\text{s}^2$) is not species-specific, but the relevance of the different discharge scenarios differs based on typical discharges during a species' migration period (see Figure 4.1). Almost all figures show that the fishway entrance is masked by turbulence, and that no continuous migration corridor exists in which the turbulence is sufficiently low (passable). The exception is scenario S100R, where all $100 \text{ m}^3/\text{s}$ is discharged by the weir farthest from the fishway.

A discharge of $100 \text{ m}^3/\text{s}$, however, bears little relevance for the migration period of glass eel (see Figure 4.1). For salmon, scenario S100R would result in a continuous migration corridor in the period July – August in terms of turbulence, but the velocities are quite low (see Section 4.2.2 and Figure 4.10). Here, the turbulence just downstream of the weir might lead the salmon towards the fishway despite the favourable velocities on the opposite side of the river, because these favourable velocities coincide with an area of high turbulence. A definitive estimation of the fishway findability in S100R is therefore quite difficult. The small turbulent area (red) in the middle of the fishway entrance should not be interpreted as problematic based on these simulations alone: the exact geometry of the fishway and the connection between fishway and riverbed is too uncertain (see Section 3.1) to draw that conclusion.

It must be noted that it is expected that the presented values of turbulent kinetic energy are conservative: Duguay et al. (2017) compared RANS simulations and acoustic Doppler velocimetry (ADV) field measurements of fishways and found that water levels and flow velocities were predicted accurately, but a difference of 30 – 40% was found for turbulent kinetic energy. Zubova et al. (2022) showed that the turbulent kinetic energy close to a structure is underestimated by STAR-CCM+'s realisable $k - \varepsilon$ model compared to particle image velocimetry (PIV) measurements in a physical scale model of an underflow weir. The turbulent kinetic energy may therefore be higher (meaning less favourable) in practice than what is shown in Figure 4.14 through Figure 4.18.

4.3.2 Vorticity

Figure 4.19 through Figure 4.23 show the horizontal and vertical vorticity downstream of weir Grave for scenarios S100, S100L, S100R, S250 and S330, respectively. Any transparent areas in the shown cross-sections indicate that the vorticity exceeds the vorticity limit $|\omega| \leq 0.3 \text{ s}^{-1}$.

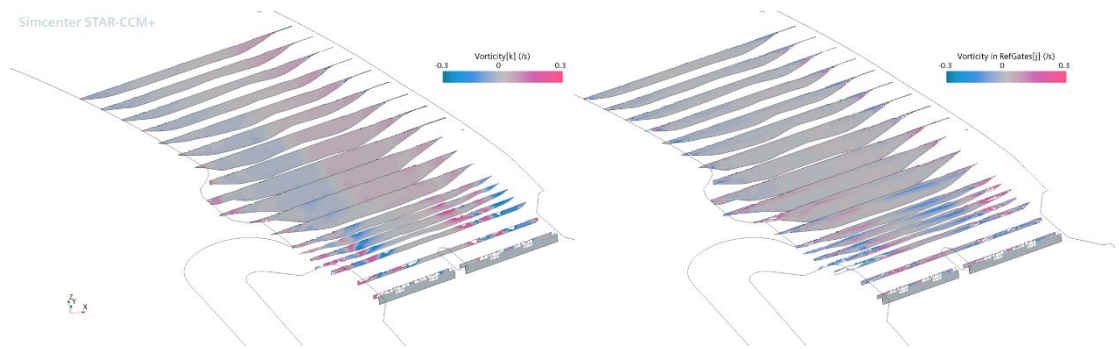


Figure 4.19: **[EN]** Vorticity in the horizontal (left) and vertical (right) plane downstream of weir Grave in scenario S100, where pink and blue indicate positive and negative vorticity, respectively. **[NL]** Vorticiteit in het horizontale (links) en verticale vlak (rechts) benedenstrooms van stuw Grave in scenario S100, waar roze (positief) en blauw (negatief) de richting aangeven.

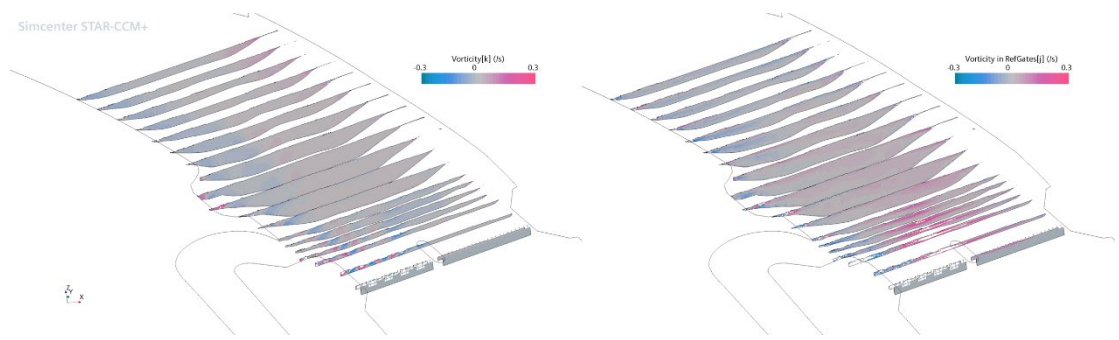


Figure 4.20: **[EN]** Vorticity in the horizontal (left) and vertical (right) plane downstream of weir Grave in scenario S100L, where pink and blue indicate positive and negative vorticity, respectively. **[NL]** Vorticiteit in het horizontale (links) en verticale vlak (rechts) benedenstrooms van stuw Grave in scenario S100L, waar roze (positief) en blauw (negatief) de richting aangeven.

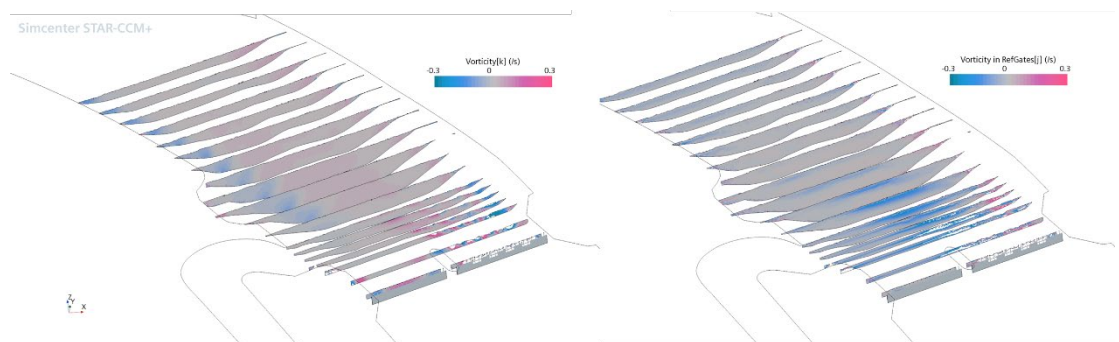


Figure 4.21: **[EN]** Vorticity in the horizontal (left) and vertical (right) plane downstream of weir Grave in scenario S100R, where pink and blue indicate positive and negative vorticity, respectively. **[NL]** Vorticiteit in het horizontale (links) en verticale vlak (rechts) benedenstrooms van stuw Grave in scenario S100R, waar roze (positief) en blauw (negatief) de richting aangeven.

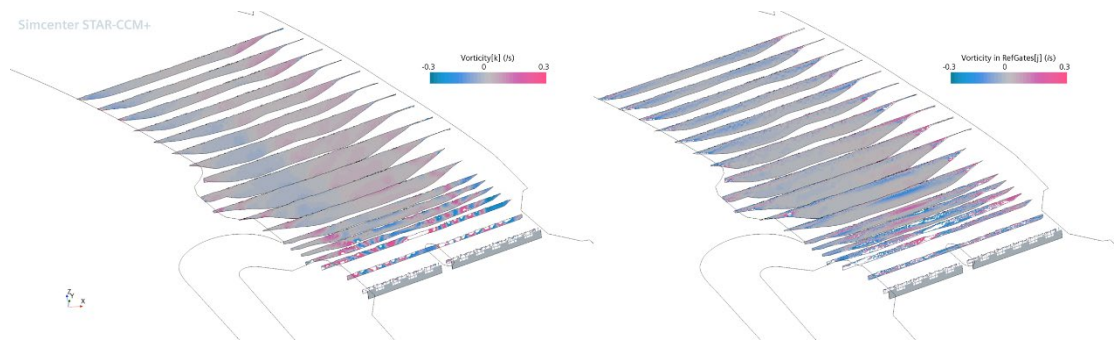


Figure 4.22: **[EN]** Vorticity in the horizontal (left) and vertical (right) plane downstream of weir Grave in scenario S250, where pink and blue indicate positive and negative vorticity, respectively. **[NL]** Vorticiteit in het horizontale (links) en verticale vlak (rechts) benedenstrooms van stuw Grave in scenario S250, waar roze (positief) en blauw (negatief) de richting aangeven.

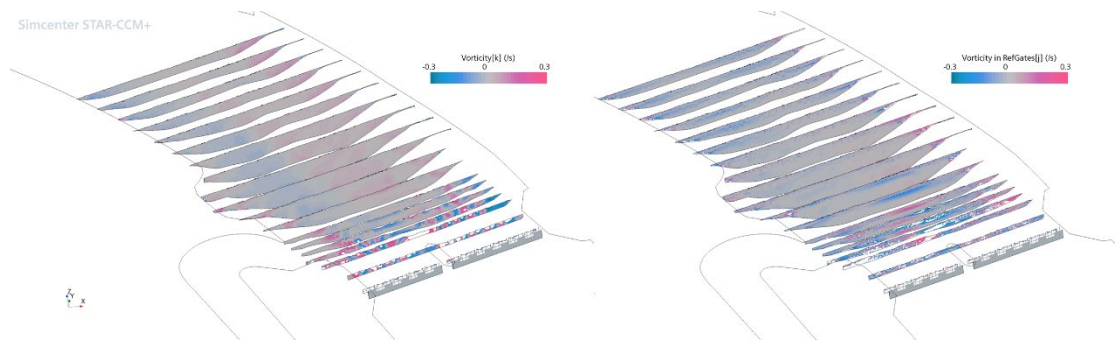


Figure 4.23: **[EN]** Vorticity in the horizontal (left) and vertical (right) plane downstream of weir Grave in scenario S330, where pink and blue indicate positive and negative vorticity, respectively. **[NL]** Vorticiteit in het horizontale (links) en verticale vlak (rechts) benedenstrooms van stuw Grave in scenario S330, waar roze (positief) en blauw (negatief) de richting aangeven.

The horizontal vorticity limit $|\omega_z| \leq 0.3 \text{ s}^{-1}$ (Marriner, et al., 2014) is not exceeded near the fishway or in the downstream section leading up to it in any of the scenarios. The limit is exceeded in-between the fishway and the weir in some of the cases, but this is not considered problematic because we do not want fish to swim beyond the entrance of the fishway.

For vertical vorticity, no limiting value was found in the literature, but the figures also use the same limit: $|\omega_y| \leq 0.3 \text{ s}^{-1}$, which is not exceeded in the region of interest. The literature suggests that in the vertical plane, particularly negative vorticity is detrimental to fish (Muhawenimana et al., 2019). There are some regions of negative vorticity in the region of interest (highlighted in blue). The vorticity magnitude does not exceed the applied vorticity limit, but the significance of this limit is currently unknown. In the asymmetrical simulations S100L and S100R, the vorticity in the vertical plane in front of the weir is directed in opposite directions, where negative vorticity results from the case with removed gates in only the farthest weir.

Only one source was found that quantified a horizontal vorticity limit, while no sources were found that quantify a vertical vorticity limit. The importance of sufficiently low vorticity, however, is quite often named in literature as an essential aspect of fish passability of structures (see Section 2.2.2). This suggests that more research on the effects of vorticity on fish is needed for a better understanding of its influence on fishway findability.

5 Conclusion

For glass eel, fishway findability at weir Grave is too low based on both flow velocity and turbulence. For salmon, a continuous migration corridor exists in terms of velocity in all scenarios except one. At 330 m³/s through the weir closest to the fishway, the CFD simulations do not show a continuous migration corridor, but from the validation with field measurements we know that the velocities in the jet were likely overestimated. The velocities may therefore be more favourable than what was shown by the CFD model. Turbulence, however, almost always disrupts the available migration routes, which is also evident from pictures that were taken during the field measurements. For $Q = 100$ m³/s, it was shown that three different weir gate configurations (that achieve that same discharge) result in different flow patterns and migration routes. This highlights the importance of weir configuration (fish-friendly weir operation) and even weir type, as different weir types offer different possibilities in terms of variability (by having few large versus many small gates over the width of the river). The interpretation of 100 m³/s through the weir farthest from the fishway turned out not to be straightforward. It is the only scenario in which the turbulence close to the fishway is sufficiently low (passable). But based on velocity, for (bottom-dwelling) glass eel only a narrow, winding path close to the water surface exists. For salmon, the velocities near the fishway are too low and favourable velocities are present on the opposite side of the river (but in a turbulent area). An overview of the findability per species, per parameter and overall, and for each discharge scenario is shown in Table 5.1.

Table 5.1: Summary of the findability of the fishway at weir Grave in the different scenarios.

		Scenario	S100	S100L	S100R	S250	S330
		Parameter					
Glass eel	Velocity		Too high	Too high	Questionable	Too high	Too high
	Turbulence		Too high	Too high	Good	Too high	Too high
	Overall		Findable: X	Findable: X	Findable: ?	Findable: X	Findable: X
Salmon	Velocity		Good	Good	Questionable	Good	Inconclusive
	Turbulence		Too high	Too high	Good	Too high	Too high
	Overall		Findable: X	Findable: X	Findable: ?	Findable: X	Findable: X

Based on the performed simulations, the findability of the fishway at weir Grave does not seem sufficient for large-scale successful upstream migration (see Table 5.1). For the future weirs in the Meuse, ecologists and hydraulic engineers must work together to determine the hydraulic conditions through which fish can most readily pass, and then translate these conditions into a successful fishway design or operation protocol. The present study has shown that CFD can be successfully applied to quantify the consequences of (hydraulic) design choices and weir operation for fishway findability.

It must be noted that glass eel and salmon could be considered lower and upper limit in terms of swimming performance in the Meuse: there are many species with swimming performances somewhere in-between. It is also very important to note that the findability or even passability of fishways does not mean that fish will thrive in the Meuse: fish also require suitable habitats and food sources in-between the weirs. Particularly rheophilic (flow-loving) fish are impacted negatively by hydraulic structures that stagnate water and prevent the river from flowing freely.

5.1 Recommendations for further research

Through performing the simulations and doing literature research, a few recommendations for further research have been identified:

- Carry out similar studies for other weir types and fishway configurations. The weirs and fishways in the Meuse are all unique in one way or another.
- Carry out a similar study for a weir in a tidal area. In an evaluation of the fishways at the weirs in the Lower Rhine and Lek, Winter (2010) suggests that fishway findability may be influenced by tidal variations. This would be relevant for weir Hagestein (Lek) and weir Lith (Meuse).
- Carry out a similar study for the preliminary design of a future weir, such as the sector gate design for weir Sambeek (Kortlever, et al., 2024). In such a design-oriented study, the ideal location of the fishway entrance could be determined.
- Quantify the findability and passability of outside-the-box weir alternatives, such as a rock ramp fishway (Cassan et al., 2023; Stuart et al., 2024; Thorncraft & Marsden, 2000).
- Perform experiments to collect (species-specific) data on the influence of turbulence on migratory fish. Turbulence is often cited as an important flow characteristic, but often has not been quantified in the literature.
- Rethink nature-like bypass fishways – can we make a design with multiple (downstream) entrances work? Designs with a bypass (upstream) are already implemented at weir Driel (Lower Rhine) and weir Hagestein (Lek). Weir Driel also has a forked fishway entrance, but this is considered sub-optimal because the attraction flow becomes too diffuse as it distributes over the two branches (Rijkswaterstaat Waterdienst, 2011).
- Apply detached eddy or large eddy simulations, as turbulence is a highly anisotropic phenomenon that is not captured well by $k - \varepsilon$ models. Research found that Reynolds' shear stress is an important parameter for fish (Silva et al., 2012; Muhawenimana et al., 2019; Odeh, et al., 2002), but this parameter cannot be captured using a two-equation model such as $k - \varepsilon$.

6 References

- Aarts, B. G., & Nienhuis, P. H. (2003). Fish zonations and guilds as the basis for assessment of ecological integrity of large rivers. *Hydrobiologia*, 500, 157-178.
- Arcadis. (2018). *Vismigratierivier Afsluitdijk - Hydraulische en ecologische toetsing van het ontwerp*.
- ATKB. (2021). *Stromend Habitat en Connectiviteit in de Maas*. 20200920/rap01.
- Baudoin, J., Burgun, V., Chanseau, M., Larinier, M., Ovidio, M., Sremski, W., . . . Voegtle, B. (2014). *Assessing the passage of obstacles by fish - Concepts, design and application*. The ICE protocol for ecological continuity.
- Bleckmann, H., & Zelick, R. (2009). Lateral line system of fish. *Integrative Zoology*, 4(1), 13-25.
- Brandl, A., Laaha, G., Käfer, S., & Mader, H. (2022). Key Factors for the Findability of Fish Passes in Large Epipotamal Rivers: The Case of the River Drava. *Water*, 14(1530).
- Cassan, L., Miranda, F. C., Laurens, P., & Courret, D. (2023). Hydraulic of rock-ramp fishway with lateral slope. *Environmental Fluid Mechanics*.
- Coenen, J., Antheunisse, M., Beekman, J., & Beers, M. (2013). *Handreiking vispassages in Noord-Brabant*. Waterschap De Dommel, Waterschap Aa en Maas & Waterschap Brabantse Delta.
- Cotel, A. J., & Webb, P. W. (2015). Living in a Turbulent World - A New Conceptual Framework for the Interactions of Fish and Eddies. *Integrative and Comparative Biology*, 55(4), 662-672.
- Daneshvar, F., Pouyan Nejadhashemi, A., Woznicki, S., & Herman, M. (2017). Applications of computational fluid dynamics in fish and habitat studies. *Ecohydrology & Hydrobiology*, 17(1), 53-62.
- Deinet, S., Flint, R., Puleston, H., Baratech, A., Royte, J., Thieme, M. L., . . . Wanningen, H. (2024). *The Living Planet Index (LPI) for migratory freshwater fishes 2024 update - Technical report*. World Fish Migration Foundation, The Netherlands.
- Deltares. (2018). *Memo 'Stroombeelden Stuw Grave bij calamiteit'*. 11200518-011-GEO-0002.
- Duguay, J., Lacey, R., & Gaucher, J. (2017). A case study of a pool and weir fishway modeled with OpenFOAM and FLOW-3D. *Ecological Engineering*, 103, 31-42.
- Flores, N., Collas, F., & Leuven, R. (2022). 3D upstream passability of novel river training structures by migratory fish in the river Waal. *Knowledge & Management of Aquatic Ecosystems*, 423(23).
- Gisen, D., Weichert, R., & Nestler, J. (2017). Optimizing attraction flow for upstream fish passage at a hydropower dam employing 3D Detached-Eddy Simulation. *Ecological Engineering*, 100, 344-353.
- ICPDR. (2013). *Measures for ensuring fish migration at transversal structures*. ICPDR – International Commission for the Protection of the Danube River.
- IUCN. (2024, 9). Retrieved from The IUCN Red List of Threatened Species: <https://www.iucnredlist.org/>
- Kortlever, W., Koedijk, O., Maijvis, S., Zubova, A., O'Mahoney, T., & ten Hove, D. (2024). To Determine the Opening Width of a Navigable Weir in the Meuse by Means of Flow and Nautical Simulations During a River Flood. *10th International Symposium on Hydraulic Structures, Zurich, Switzerland, 17-19 June 2024*.
- KpNK. (2022). *Analyse naar de doorvaarbaarheid van de toekomstige Maasstuwen*. 11208384-002-HYE-0001.
- Kroes, M., & Monden, S. (2005). *Vismigratie: Een handboek voor herstel in Vlaanderen en Nederland*. Brussel: Ministerie van de Vlaamse Gemeenschap. AMINAL, Afdeling Water.

- KRW. (2000). Richtlijn 2000/60/EG van het Europees Parlement en De Raad van 23 oktober 2000 tot vaststelling van een kader voor communautaire maatregelen betreffende het waterbeleid. *Publicatieblad van de Europese Gemeenschappen*.
- Larinier, M. (2002). Fishways: biological basis, design criteria and monitoring. *Bull. Fr. Pêche Piscic.*, 28-38, 39-53.
- Lauder, B., & Spalding, D. (1974). The numerical computation of turbulent flows. *Computer Methods in Applied Mechanics and Engineering*, 3(2), 269-289.
- Li, G., & Zheng, T. (2009). Optimizing the entrance location for a fish pass facility with limited attraction flow in a large river - A case study of the Jinsha River, China. *Canadian Journal of Engineering*.
- Marriner, B., Baki, A., Zhu, D., Thiem, J., Cooke, S., & Katopodis, C. (2014). Field and numerical assessment of turning pool hydraulics in a vertical slot fishway. *Ecological Engineering*, 63, 88-101.
- Muhawenimana, V., Wilson, C. A., Ouro, P., & Cable, J. (2019). Spanwise Cylinder Wake Hydrodynamics and Fish Behavior. *Water Resources Research*, 8569-8582.
- NASA. (2021, February 10th). *Examining Spatial (Grid) Convergence*. Retrieved July 29th, 2024, from NPARC Alliance CFD Verification and Validation Web Site: <https://www.grc.nasa.gov/www/wind/valid/tutorial/spatconv.html>
- Odeh, M., Noreika, J., Haro, A., Maynard, A., Castro-Santos, T., & Cada, G. (2002). *Evaluation of the effects of turbulence on the behaviour of migratory fish*. BPA Report DOE/BP-00000022-1.
- Pavlov, D. (1989). *Structures assisting the migration of non-salmonid fish: USSR*. Severtsov's Institute of the Evolutionary Morphology and Ecology of Animals - FOA Fisheries Technical Paper 308.
- Platform Rivierkennis. (2018). *Het verhaal van de Maas - De Maas uit balans?*
- Redeker, M., & Heimerl, S. (2018). Improved Fish Pass Entrance Involving Surplus Attraction Flow. *7th International Symposium on Hydraulic Structures, Aachen, Germany, 15-18 May 2018*.
- Rijkswaterstaat. (2011). *Sluis- en Stuwcomplex in de Maas - Sluis/Stuwcomplex Grave*. Inspectietekeningenset 45F-001-07.
- Rijkswaterstaat. (2022b). *Vervanging en Renovatie. Prognoserapport 2022. Prognose voor de periode 2023 tot en met 2050*.
- Rijkswaterstaat. (2023a). *Stuwen in de Maas - Systeembeschouwing*. CON00-1663636127-39 v1.0.
- Rijkswaterstaat. (2023b). *Objectbeschrijving sluis- en stuwcomplex Grave*.
- Rijkswaterstaat Waterdienst. (2011). *Hydraulische metingen vispassages Nederrijn-Lek. Resultaten 2002-2007*.
- Roache, P. (1994). Perspective: A Method for Uniform Reporting of Grid Refinement Studies. *Journal of Fluids Engineering*, 116(3), 405-413.
- Sagarin, R., & Pauchard, A. (2012). *Observation and Ecology - Broadening the Scope of Science to Understand a Complex World*. Washington, DC: Island Press.
- Siemens. (2021). *Simcenter STAR-CCM+ 2021.2 (16.04.007-R8) Documentation*. Siemens.
- Silva, A., Katopodis, C., Santos, J., Ferreira, M., & Pinheiro, A. (2012). Cyprinid swimming behaviour in response to turbulent flow. *Ecological Engineering*, 44, 314-328.
- STOWA. (2009). *Handboek Debietmeten in Open Waterlopen*. Rapportnummer 2009-41.
- Stuart, I. G., Marsden, T. J., Jones, M. J., & Moore, M. T. (2024). Rock fishways: Natural designs for an engineered world. *Ecological Engineering*, 206.
- Tarrab, L., García, C. M., Cantero, M. I., & Oberg, K. (2012). Role of turbulence fluctuations on uncertainties of acoustic Doppler current profiler discharge measurements. *Water Resources Research*, 48.
- Thorncraft, G., & Marsden, T. (2000). *Rock-ramp Fishway Design Principles*. Queensland Fisheries Service.

- Tritico, H. M., & Cotel, A. J. (2010). The effects of turbulent eddies on the stability and critical swimming speed of creek chub (*Semotilus atromaculatus*). *The Journal of Experimental Biology*, 213, 2284-2293.
- Van Daal-Rombouts, P., Tralli, A., Verhaart, F. L., & Clemens, F. (2014). Applicability of CFD modelling in Determining Accurate Weir Discharge-Water Level Relationships. *13th International Conference on Urban Drainage, Sarawak, Malaysia, 7-12 September 2014*.
- Veza, P., Libardoni, F., Manes, C., Tsuzaki, T., Bertoldi, W., & Kemp, P. S. (2020). Rethinking swimming performance tests for bottom-dwelling fish: the case of European glass eel (*Anguilla anguilla*). *Scientific Reports*.
- Williams, J., Armstrong, G., Katopodis, C., Larinier, M., & Travade, F. (2011). Thinking like a Fish: A Key Ingredient for Development of Effective Fish Passage Facilities at River Obstructions. *River Research and Applications*, 28, 407-417.
- Winter, H. V. (2010). *Evaluatie van de vistrappen in de Nederrijn-Lek*. IMARES - Institute for Marine Resources & Ecosystem Studies, Wageningen UR - Rapportnummer C064/10.
- Winter, H. V., Griffioen, A. B., & van Keeken, A. (2014). *De Vismigratierivier: Bronnenonderzoek naar gedrag van vis rond zoet-zout overgangen*. IMARES - Institute for Marine Resources & Ecosystem Studies (Wageningen UR).
- WL | Delft Hydraulics. (2006). *Efficiëntere vismigratie bij vistrappen en kunstwerken - Onderzoek op vismigratie gericht stuwbeheer in de Maas bij Sambeek*. Q4092.
- Wolter, C., & Arlinghaus, R. (2004). Burst and critical swimming speed of fish and their ecological relevance in waterways. *Annual Report 2003 Leibniz-Institute of Freshwater Ecology and Inland Fisheries*, 77-93.
- Zubova, A., Oldenziel, G., & O'Mahoney, T. (2022). PIV Measurements and CFD Modeling for Verification of the Turbulent Flow Downstream of an Underflow Gate. *Proceedings of the 39th IAHR World Congress, 19–24 June 2022, Granada, Spain*, 2786-2796.

Deltares is een onafhankelijk kennisinstituut voor toegepast onderzoek op het gebied van water en ondergrond. Wereldwijd werken we aan slimme oplossingen voor mens, milieu en maatschappij.

Deltares

www.deltares.nl